

# JOMCOM

**Journal of Millimeterwave Communication,  
Optimization and Modelling**

editor in chief

**Assoc. Prof. M. Tahir GUNESER**

**Volume :** 3

**Issue :** 1

**Year :** 2023

**ISSN :** 2791-9293

**CONTENT**

Content	i
About the Journal	ii
Editor in Chief	ii
Publisher	ii
Aims & Scope	iii
 1. A Quantum Machine Learning Approach for Detecting User Locations <i>Erkan Güler, M. Talha Kakız, Tuğrul Çavdar, F.Baturalp Günay, Burcu Şanal</i>	 <u>1-8</u>
 2. Wireless Communication Between Vehicles: Exploring the Potential of V2V and V2X Communication for Improved Efficiency, Safety, and Sustainability <i>Muhammed Alsudani</i>	 <u>9-13</u>
 3. Maximum Power Point Tracking Achievements and Challenges in Photovoltaic Systems: Review <i>Ahmed Mousay</i>	 <u>14-20</u>
 4. The Viability and Cost-Effectiveness of Hybrid Renewable Energy Systems in Rural Areas <i>Abdullah Abodwair</i>	 <u>21-26</u>
 5. Using ANFIS to Predict the Long and Short Term Stroke Risk Based on Ultrasound Carotid Imaging and Clinical data of Initially Asymptomatic Patients <i>Suahil Odeh, Efthymoulos Kyriacou, Constantinos S. Pattichis</i>	 <u>27-31</u>

## About the Journal

Journal of Millimeterwave Communication, Optimization and Modelling (JOMCOM) is an international on-line and refereed journal published 2 times a year (June and December) in English.

Journal of Millimeterwave Communication, Optimization and Modelling (JOMCOM) published its first issue in 2021 and has been publishing since 2021. Manuscripts in JOMCOM Journal reviewed of at least 2 referees among the referees who have at least doctorate level in their field.

Journal of Millimeterwave Communication, Optimization and Modelling (JOMCOM) is an international online journal that is published 2 times in a year in English.

The purpose of JOMCOM is publishing the scientific research in various fields of communication.

All kinds of transactions and the application about the journal can be made from <https://jomcom.org>

The scientific responsibility of articles belongs to the authors.

ISSN: 2791-9293

## Editor in Chief:

**Assoc. Prof. Dr. Muhammet Tahir GÜNEŞER**

Karabük University

Faculty of Engineering

Department of Electrical and Electronics Engineering

Head of Communication Division

Karabük, TURKEY

jomcomeditor@gmail.com

## PUBLISHER

Assoc. Prof. Muhammet Tahir GÜNEŞER

## Aims & Scope

Communication Technologies: Journal of Millimeter-wave Communication, Optimization and Modelling (JOMCOM) publishes original research and review articles in Communication Technologies, Innovative Technologies, and Systems in the broad field of Information-Communication Technology. Purpose of JOMCOM; To create value in the field by publishing original studies that will contribute to the literature in wireless communication sciences and be a resource for academia and industrial application whole over the world. Besides, JOMCOM aims to bring the valuable work of researchers working in Communication studies to a broader audience at home and abroad. Readership of JOMCOM; valuable representatives of the wireless communication area, especially those who do academic studies in it, and those who do academic studies about modelling and system design and other interested parties. Since JOMCOM will appeal to a broader audience in article submissions, it prioritizes studies prepared in English.

Optimization and Modelling: Journal of Millimeter-wave Communication, Optimization and Modelling (JOMCOM), within the scope of Wireless Communication Sciences, publishes articles on communication theory and techniques, systems and networks, applications, development and regulatory policies, standards, and management techniques. It also reports experiences and experiments, best practices and solutions, lessons learned, and case studies. Additional studies on System Design, Modelling and Optimization. Subject areas of interest covered in the journal include the following but are not limited to:

5G-6G Technologies

Circuits for Optical Communication Systems

Antenna Design

Communication Design Materials

Fiber Optic Communication

Innovative Designs for Communications

Integrated Circuits for Communications

Optimization Methods on Engineering

Realization of Antenna Systems

Realization of Microwave, Radar, and Sonar Systems

RF Circuits

System Design

Visible Light Communication

Wireless Communication

# A Quantum Machine Learning Approach for Detecting User Locations

Received: 30 February 2023; Accepted: 5 March 2023

Research Article

Erkan Güler

Department of Computer Engineering  
Giresun University  
Giresun, Türkiye  
erkan.guler@giresun.edu.tr  
ORCID: 0000-0001-7225-0859

Muhammet Talha Kakız

Department of Computer Engineering  
Osmaniye Korkut Ata University  
Osmaniye, Türkiye  
mtalhakakiz@osmaniye.edu.tr  
ORCID: 0000-0003-4928-6559

Tuğrul Çavdar

Department of Computer Engineering  
Karadeniz Technical University  
Trabzon, Türkiye  
ulduz@ktu.edu.tr  
ORCID: 0000-0003-3656-9592

Faruk Baturalp Günay

Department of Computer Engineering  
Atatürk University  
Erzurum, Türkiye  
baturalp@atauni.edu.tr  
ORCID: 0000-0001-5472-3608

Burcu Şanal

Vocational School of Technical  
Sciences  
Recep Tayyip Erdoğan University  
Rize, Türkiye  
burcu.sanal@erdogan.edu.tr  
ORCID: 0000-0002-4541-7622

**Abstract**—Quantum Machine Learning methods are becoming a key component for various types of tasks making predictions or decisions based on datasets. Recent efforts and researches on quantum computing point out the significance of quantum speedup advantage, especially for learning processes that require enormous amount of computational resources. Advances in both quantum hardware design and hybrid quantum-classical software frameworks accommodate a paradigm shift from classical to quantum. In consideration with this quantum leap notion, we investigate the capability of variational quantum algorithms (VQA) on a real world problem of user localization dealing with the binary classification task. This paper introduces a VQA with four variants that differ in the number of layers related to the variational quantum circuit (VQC) part of the VQA. The samples from a publicly available user localization dataset are first preprocessed through padding, scaling and normalization. Next, they are mapped into three qubit quantum states using amplitude encoding as a data embedding scheme. Unitary transformation of the mapped quantum data in the VQC is followed by a measurement in computational basis to produce predictions for the labels. The error between true and predicted labels is computed in a classical manner and a cost function minimization process is executed with the aid of gradient descent algorithm. The updated training parameters from the optimization stage are fed into the VQC and this process is repeated until the learnable parameters converge. The simulation results demonstrate that the designed VQA for binary classification achieves an accuracy value of 99% in the training phase. Moreover, the ratio of predicted labels to true labels approaches to 93% during the validation of actual user locations based on the signal strength received from the routers that are positioned at different places in a facility.

**Keywords**—quantum machine learning, user localization, variational quantum algorithm, variational quantum circuit, amplitude encoding

## I. INTRODUCTION

Quantum computing is a fascinating computer science field that has attracted the attention of scientists and professionals from various disciplines. Although the intense curiosity might be reasoned in a variety of ways, the foremost

argument that can be raised against the profound interest in this emerging technology is twofold: (1) Current methods in producing classical computers are in the eve of encountering size related problems. As electronic devices get smaller, quantum effects start to influence the precise functioning of computers [1]. (2) Quantum computation is proved to be much more efficient than its classical counterpart for some computational tasks of practical importance such as integer factorization [2], search for an element in unstructured database [3] and simulation of quantum systems [4].

The massive computational power of quantum computers has led major IT companies (e.g., IBM, Google, and D-Wave) to produce quantum hardware, some of which are exposed via cloud platforms. However, currently available quantum computers are in infancy period suffering from environmental noise and it is the major difficulty in building large-scale quantum computers [5]. Noise causes disturbances in the state of the basic information unit *quantum bit* (qubit) and affects the computational accuracy. Due to the issue of noise, the current state of the art in the fabrication of quantum processors is described as Noisy Intermediate Scale Quantum (NISQ) era [6], where intermediate scale refers to the qubit number used in quantum computers varying from 50 to a few hundred qubits. With the introduction of NISQ devices, researchers have started to investigate the potential uses of quantum computers in various fields including finance, robotics, cybersecurity, energy management and chemical engineering [7]. Among all the research areas in relation to the quantum computing, the quantum machine learning (QML) is one of the most promising one [8] and has become an active subfield of quantum computing research [9].

The main goal of Machine Learning (ML), which spans a wide range of disciplines and has numerous applications, is to learn from data. Statistical patterns in data are recognized and inferences are drawn during the learning process. Despite advances in GPUs for parallel processing, the volume of data generated recently exceeds the computational power of conventional computers [10]. Thus, quantum computing has opened up a new playground for machine learning namely QML, which investigates the approaches and methods that

harness the fields of machine learning and quantum computing [11]. Researchers are focused on using the power of quantum computers to solve machine learning problems at considerably faster rates than classical counterparts [12] with the aid of QML.

Variational quantum algorithms (VQA), also referred to as hybrid quantum-classical algorithms, are described as encouraging approaches that employ NISQ devices to perform QML and to address real world problems that are beyond the capabilities of classical computers [13]. Variational Quantum Eigensolver and Quantum Approximate Optimization Algorithm are examples of the VQA algorithms. In this framework, computational tasks are split between quantum and classical resources. The quantum part of the framework employs parameterized (variational) quantum circuits to predict the labels of the training data through approximations. On the other hand, the classical part iteratively executes the update routines for the parameters of the parametrized quantum circuit (PQC) [14]. The functionality of these parameters bears resemblance to the weights of an artificial neural network. The fault-tolerant quantum computers are still an open research issue. However, the effect of noise on NISQ devices can be mitigated by keeping the circuit depth shallow [15]. This strategy provides an advantage for the QML methods using PQCs.

ML methods are broadly grouped under three different types: Supervised learning, unsupervised learning and reinforcement learning. In this work, we address one of the ML methods, which is binary classification as a supervised learning approach. We aim at supplying the practical implementation of required QML-based classification method by tackling a problem known as user localization in an indoor environment. Also, we investigate the layered structure of the utilized VQC in the context of improved classification outcomes.

This paper is organized as follows: We give a brief literature overview in Section II. The background about the concepts of quantum computation and quantum circuits is covered in Section III, while Section IV deals with the proposed quantum circuit for the classification problem. The results and the corresponding interpretations are drawn in Section V. We conclude the paper with summary and future research directions in Section VI.

## II. RELATED WORK

The authors of [16] propose a model for the indoor localization of users in a building. The Received Signal Strength Indicator (RSSI) data gathered from the user equipments is exploited to perform an estimation on indoor occupancy count. The occupancy issue is handled as a binary classification problem, for which the following machine learning algorithms are used: k-nearest neighbor, decision tree, support vector machine and logistic regression. Recurrent neural networks are also studied in regard to locating people or objects within a building. The research presented in [17] focuses on a learning algorithm named as Speed Conscious Recurrent Neural Network, which provides a way to predict the locations. Furthermore, the authors propose fault-tolerant approaches such as nearest RSSI and most recent RSSI with the aim of improving the location accuracy.

In [18], remote health monitoring and smart homes are stated as some of the IoT applications, which are in need of

location estimation techniques. The authors introduce a device-free localization system consisted of passive infrared (PIR) sensors. The data collected through PIR sensors is evaluated with deep learning algorithms such as convolutional neural networks and recurrent neural networks in order to estimate the user locations. Variances in received signal strength from user terminals, device heterogeneity and environment complexity such as obstacles in a building can cause challenges on the localization problem. Due to this fact, the work in [19] introduces a high adaptability indoor localization method using a backpropagation neural network. The devised approach reveals the similarities on the received signal strength fingerprints and provides an improved localization accuracy.

One of the first researches related to classification problem using quantum computers is included in [20]. The authors exploit the idea of Hamming Distance measurement on a quantum computer in order to classify the handwritten digits from the well-known MNIST dataset.

As an effort of adapting the deep neural networks into the quantum realm, the work in [21] introduces a variational quantum deep neural network model for the problem of image classification. The proposed three classifiers are executed on both a simulation platform and a quantum hardware. The experimental results for the binary classification of the handwritten digits in the MNIST database achieved an accuracy of 100%, while ten-label classification task for the RGB images from the UCI database obtained an accuracy rate of 91%.

It is obvious that the earlier implementations of QML algorithms have mainly benefited from the MNIST images. The advances in the parametrized quantum circuits have led the researchers to investigate the potential of PQCs for other disciplines such as geoscience and medicine. In [22], the classification of satellite images is investigated. The experimental results show that the employed PQC performs better than a classic deep learning method. The effort of malaria disease diagnosis with the aid of quantum machine learning presented in [23] is one of the first instances delving into the detection of parasites that cause lethal illnesses. The work mainly focuses on the recognition of the malaria parasites by identifying the dots on the red blood cell images. The developed classification scheme emphasizes the significance of disease detection with fewer learnable parameters and features. The issue on the reduction of training parameters is also investigated by the authors of [24]. In comparison to the classical machine learning approaches, variational quantum circuit architecture is stated to pose an advantage in terms of parameter size.

As can be seen, majority of the classification approaches in the field of quantum machine learning is about image classification, which is also intensively discussed in classical supervised learning context. However, it is crucial to attempt broadening the implementation domain of parametrized quantum circuits by taking the real world samples other than images into consideration.

## III. BACKGROUND

### A. Quantum Bit (Qubit)

The information in classical computation is represented by bits, where one bit can be in one of the two states: 0 or 1. On the other hand, the basic unit of information in quantum

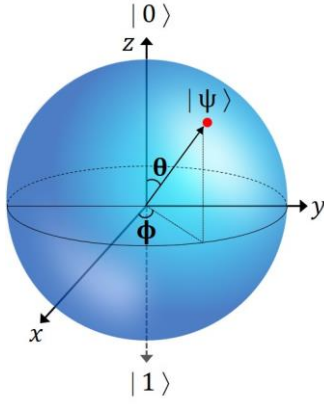


Fig. 1. Geometric representation of a qubit on Bloch Sphere

computation is qubit. A qubit can be considered as a two-level system spanned by two orthogonal states. By definition, two states are said to be orthogonal if their inner product is equal to the scalar value 0. In a 1-qubit system, those states satisfying the orthogonality condition form a basis known as computational basis and are denoted by:

$$|0\rangle = \begin{bmatrix} 1 \\ 0 \end{bmatrix}, |1\rangle = \begin{bmatrix} 0 \\ 1 \end{bmatrix} \quad (1)$$

The notation  $|\cdot\rangle$  describing the state of a quantum system is a shorthand for writing the column vectors and referred to as *ket notation*. A generic qubit state  $|\psi\rangle$  can be in a *superposition* of the computational basis states and is formulated as a linear combination of  $|0\rangle$  and  $|1\rangle$ :

$$|\psi\rangle = \alpha|0\rangle + \beta|1\rangle = \begin{bmatrix} \alpha \\ \beta \end{bmatrix} \quad (2)$$

where  $\alpha, \beta$  are complex numbers and the amplitudes of the state  $|\psi\rangle$ . Since each state vector is a unit vector in a complex vector space named as Hilbert space, the following condition must hold:

$$|\alpha|^2 + |\beta|^2 = 1 \quad (3)$$

Hence, each state  $|\psi\rangle$  has to be normalized according to the given formula above. When a state is measured in the computational basis, it collapses into either  $|0\rangle$  state with a probability of  $|\alpha|^2$  or  $|1\rangle$  state with a probability of  $|\beta|^2$ . The measurement in a quantum system changes the state implying that the original information is lost.

The utmost power of quantum computation is based on (2) due to the fact that each qubit is represented by two complex amplitudes, which are theoretically capable of taking infinitely many different values. As a consequence, a quantum system with  $n$  qubits is specified by  $2^n$  amplitudes providing a natural way of storing and manipulating enormous amount of information simultaneously, usually referred to as *quantum parallelism*. The generalization of a 1-qubit state  $|\psi\rangle$  to  $n$ -qubits is as follows:

$$|\psi\rangle = \sum_{i=0}^{2^n-1} \alpha_i |i\rangle \quad (4)$$

where the normalization conditions is satisfied:

$$\sum_{i=0}^{2^n-1} |\alpha_i|^2 = 1, \quad \alpha_i \in \mathbb{C} \quad (5)$$

A qubit can be geometrically visualized on the surface of a 3-dimensional unit sphere called as Bloch Sphere (Fig. 1). The state  $|\psi\rangle$  is associated with two spherical coordinates and its ket notation from (2) can be rewritten in terms of  $\theta$  and  $\phi$ :

$$|\psi\rangle = \cos\left(\frac{\theta}{2}\right)|0\rangle + e^{i\phi} \sin\left(\frac{\theta}{2}\right)|1\rangle \quad (6)$$

### Quantum Gates

Classical bits are altered with logical gates. The number of bits that are manipulated depends on the type of deployed gate. For instance, NOT gate operates on only one bit flipping the input bit, whereas two bits are fed into the AND gate and the result is only one bit. Note that the classical logical gates are not reversible at all. It is obvious that it is not possible to deduce the input bits of an AND gate from the output bit.

Just like the logical gates, the transformation of qubits are realized through quantum gates. Quantum gates can operate on single or multiple qubits preserving the length. In other words, they perform unitary operations so that the norm of the new output state is 1. Thus, a generic quantum gate provides a way of doing unitary transformations on a state  $|\psi\rangle$  and of producing an output state  $|\psi'\rangle$ :

$$|\psi'\rangle = U |\psi\rangle \quad (7)$$

where  $U$  denotes a unitary gate satisfying the following condition:  $UU^\dagger = I$ . The matrix multiplication of  $U$  with its conjugate transpose  $U^\dagger$  is equal to the identity matrix  $I$ . From the last statement, it can be deduced that it is possible to represent the quantum gates with matrices. So, (7) can be reformulated as matrix operations:

$$\begin{bmatrix} \alpha' \\ \beta' \end{bmatrix} = \begin{bmatrix} u_{00} & u_{01} \\ u_{10} & u_{11} \end{bmatrix} \begin{bmatrix} \alpha \\ \beta \end{bmatrix}, \quad u_{ij} \in \mathbb{C} \quad (8)$$

One of the most frequently used single-qubit quantum gate is X gate, which simply flips the state of the qubit. There also exist parametrized single-qubit gates such as RX, RY and RZ gates, which are the building blocks of variational quantum circuits. Each of those gates can manipulate the qubit state through a rotation of a specified angle  $\theta$  around the corresponding axis. On the other hand, CNOT is a two-qubit gate, where one of the qubits is the control qubit and the other one is the target qubit. As long as the control qubit is in state  $|1\rangle$ , the target qubit is flipped. The graphical representations and the corresponding matrices for X, RY and CNOT gates are given in Table I.

TABLE I. FREQUENTLY USED QUANTUM GATES AND THEIR REPRESENTATIONS

Quantum Gate as a Matrix	Graphical Representation
$X = \begin{bmatrix} 0 & 1 \\ 1 & 0 \end{bmatrix}$	
$R_y(\theta) = \begin{bmatrix} \cos(\frac{\theta}{2}) & -\sin(\frac{\theta}{2}) \\ \sin(\frac{\theta}{2}) & \cos(\frac{\theta}{2}) \end{bmatrix}$	
$CNOT = \begin{bmatrix} 1 & 0 & 0 & 0 \\ 0 & 1 & 0 & 0 \\ 0 & 0 & 0 & 1 \\ 0 & 0 & 1 & 0 \end{bmatrix}$	

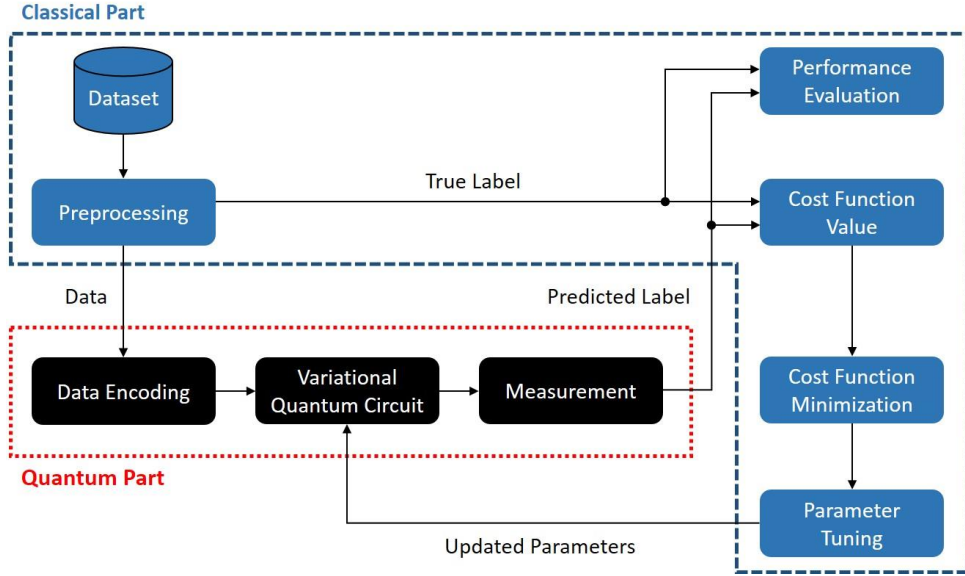


Fig. 2. Schematic representation of a variational quantum algorithm

### B. Variational Circuits

As a machine learning model, variational quantum algorithms are comprised of quantum and classical computational resources, where the former includes the variational quantum circuits. This scheme introduces a hybrid quantum-classical approach in order to perform supervised learning tasks such as classification and regression. The main steps of a variational quantum algorithm depicted in Fig. 2 are as follows:

- Data preprocessing
- Mapping of data into a quantum state
- Transformation of the quantum state with a variational quantum circuit
- Generation of a predicted value through measurement
- Comparison of the predicted label and the true label using a cost function.
- Parameter tuning through optimization of the cost function
- Performance evaluation

## IV. METHODOLOGY

In this section, the proposed variational quantum circuit is explained that is a part of the variational quantum algorithm. First of all, the employed dataset and its ingredients are introduced. The issues of scaling and normalization are the next steps before the features of a sample in the dataset are mapped into a quantum state. After the unitary transformation of the prepared quantum state is detailed, the cost function optimization will be described.

### A. Dataset

This work utilizes a publicly available dataset [25, 26] obtained by observing the signal strengths of Wi-Fi routers positioned at different locations of a facility. Each sample in the dataset constitutes of seven signal values from the routers and a label corresponding to a location in the facility. In total, there are four labeled locations, each of which are numbered

through 1 to 4 and there exist 500 samples for each of the classes. Some samples from the dataset are given in Table 2.

TABLE II. SAMPLE INSTANCES FROM THE DATASET

Router 1	Router 2	Router 3	Router 4	Router 5	Router 6	Router 7	Class
-63	-52	-56	-59	-66	-80	-80	1
-38	-55	-57	-41	-66	-73	-69	2
-51	-53	-54	-53	-62	-83	-82	3
-61	-52	-48	-61	-45	-90	-88	4

The location of a user possessing a mobile device is determined via monitoring the above mentioned router signals. Although the original dataset contains four different classes, we will be dealing with a binary classification task. So, we have only extracted class 1 and class 2 samples from the dataset.

### B. Data Preprocessing

The mentioned dataset  $\mathcal{D}$  having  $m$  samples is a set of tuples  $(x^{(i)}, y^{(i)})$ , where  $x^{(i)}$  denotes the feature vector and  $y^{(i)}$  is the corresponding label for the  $i^{th}$  sample. There exist seven features in each sample and every feature in the feature vector  $x^{(i)} = [x_1^{(i)}, x_2^{(i)}, \dots, x_7^{(i)}]^T$  is transformed by scaling it into the range  $[0,1]$  with the following min-max scaler:

$$x_j^{(i)} = \frac{x_j^{(i)} - \min_j X}{\max_j X - \min_j X}, 1 \leq j \leq 7 \quad (9)$$

where  $X = \{x^{(i)}\}_{i=1}^M$ ,  $\min_j X$  and  $\max_j X$  are the minimum and maximum of the  $j^{th}$  attribute in  $X$ , respectively;  $M$  is the number of samples in the dataset  $\mathcal{D}$ .

Since the quantum states have norm 1, before mapping the features into a quantum state, the scaled feature vector  $x^{(i)}$  has to be normalized to unit length by updating each feature  $x_j^{(i)}$  of  $x^{(i)}$  (for the simplicity of the notation, the upperscript  $(i)$  in  $x_j^{(i)}$  is omitted in the following equation):

$$x_j = \frac{x_j}{\sqrt{\sum_{k=1}^7 x_k^2}} \quad (10)$$

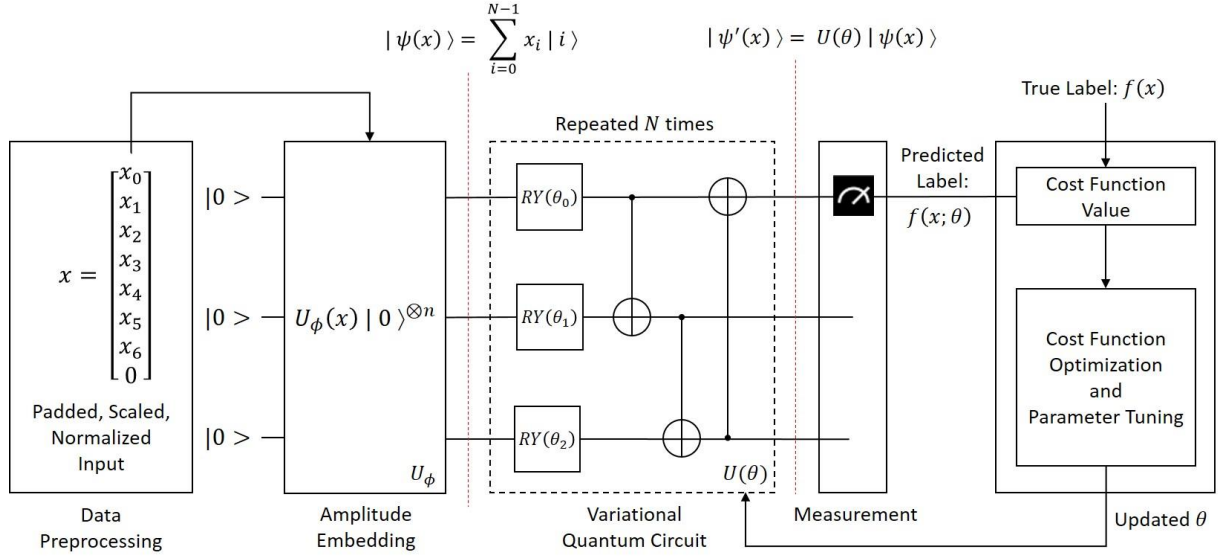


Fig. 3. Variational quantum algorithm applied on the user localization dataset

### C. Data Encoding

A feature map used in classical machine learning approaches is a function  $\phi$  that maps the data vectors in an input domain  $\mathcal{X}$  to a feature space domain  $\mathcal{X}'$ . The transformation of  $\phi: \mathcal{X} \rightarrow \mathcal{X}'$  provides a better way of representing and manipulating data while dealing with supervised learning tasks. A similar approach is also available for quantum machine learning and is called as quantum feature map. The main logic behind a quantum feature map  $\phi: x \in \mathcal{X} \rightarrow |\psi(x)\rangle \in \mathcal{H}$  is to transform the classical data into a quantum state, where the quantum state is described as a complex vector in the Hilbert space  $\mathcal{H}$  (see Section III.A). This mapping is in fact a unitary operation  $U_\phi(x)$  applied on the initial state  $|0\rangle^{\otimes n}$  using the vector  $x$ , where  $|0\rangle^{\otimes n}$  denotes the tensor product of  $n$ -qubit  $|0\rangle$  states.

Amplitude encoding [27] is one of the data encoding schemes in order to associate the classical data with the probability amplitudes of a quantum state. Supposing that the scaled and normalized feature vector  $x = [x_0, \dots, x_{N-1}]$  is real and of dimension  $N$  satisfying the condition  $2^n = N$ , the amplitude encoding can be formally described as:

$$U_\phi(x): x \in \mathbb{R}^N \rightarrow |\psi(x)\rangle = \sum_{i=0}^{N-1} x_i |i\rangle \quad (11)$$

Here,  $|i\rangle$  is the  $i^{th}$  computational basis state encoded in binary format. It has to be noted that the size of the feature vector in the user localization dataset is 7 and therefore all of the vectors have to be padded with a 0 so that the vector size is equated to an amplitude of 2. A further and important implication from the last statement is that the number of qubits required for amplitude encoding is  $\lceil \log_2 N \rceil$ .

### D. Proposed VQC and Measurement Process

The main component of a VQA is the variational quantum circuit transforming the encoded input state  $|\psi(x)\rangle$  into a new state  $|\psi'(x)\rangle$ . The parameter  $\theta$  in the proposed VQC (Fig. 3), which is a vector of trainable parameters, is evolved during the learning phase. The unitary transformation  $U(\theta)$  applied

on  $|\psi(x)\rangle$  is composed of the following gates: 1-qubit parametrized RY rotation and 2-qubit CNOT gates that provide the entanglement between the qubits in the circuit. The used VQC in this work is cascaded as multiple layers in order to allow the learning model to fit more complex functions and it is repeated  $N$  times in the QML model. The functionality of a VQC is formally described as:

$$|\psi'(x)\rangle = U(\theta) |\psi(x)\rangle \quad (12)$$

where  $\theta = [\theta_1, \theta_2, \dots, \theta_m]$  and  $m$  is the number of parameters in the VQC.

The qubits in the circuit are numbered in a sequential manner from top to down. The top qubit is referred to as the least significant qubit. It is measured in the computational basis that is also known as a Pauli-Z measurement. Depending on the fact that the eigenvalues of the Pauli-Z gate are -1 and 1, the obtained measurements results are associated to continuous values in the range from -1 to 1.

The operator used in the measurement process is the observable  $\hat{B}$  of the quantum circuit. The expectation value  $f(x; \theta)$  out of the measurement is the counterpart of the predicted label in the classical machine learning:

$$f(x; \theta) = \langle \psi'(x) | \hat{B} | \psi'(x) \rangle \quad (13)$$

Since the labels of the dataset are discrete values for the classification task (e.g., 1 for class 1 and 2 for class 2), the value of  $f(x; \theta)$  has to be adjusted accordingly:

$$f(x; \theta) = \begin{cases} 1 & \text{if } f(x; \theta) < 0 \\ 2 & \text{if } f(x; \theta) \geq 0 \end{cases} \quad (14)$$

### E. Postprocessing

The task of postprocessing is executed on the classical part of the variational quantum algorithm. Firstly, the predicted label and true label are passed to a cost function in order to quantify the error between the predicted and actual outcomes. This work utilizes the Mean Squared Error (MSE) as the cost function:

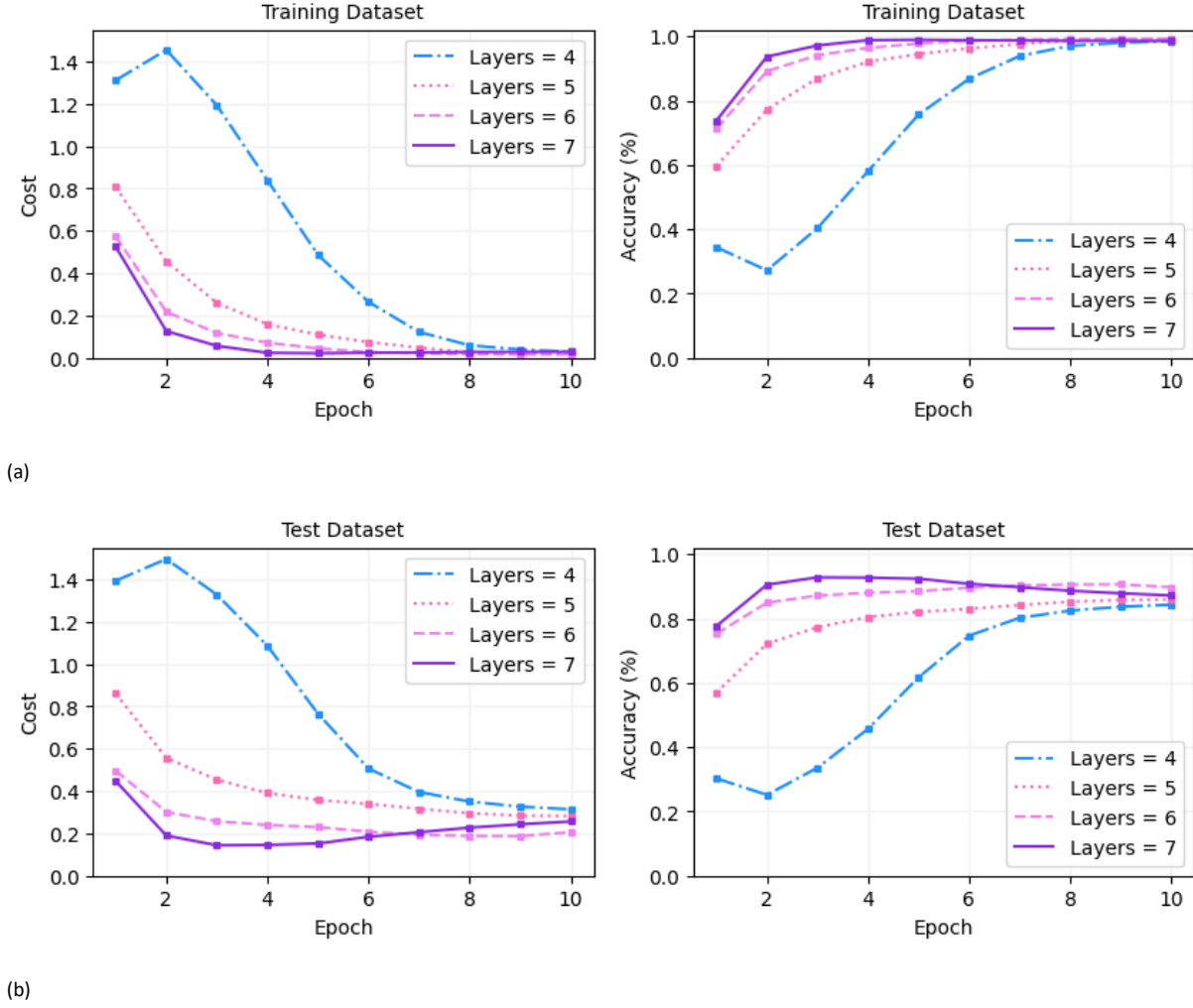


Fig. 4. Performance of the VQAs with different number of layers used in the corresponding VQCs. (a) Cost and accuracy values obtained for the training dataset. (b) Cost and accuracy values obtained for the test dataset.

$$J(\theta) = \frac{1}{2M} \sum_{i=1}^M (f(x^{(i)}; \theta) - f(x^{(i)}))^2 \quad (15)$$

where  $x^{(i)}$  is the  $i^{th}$  sample in the dataset  $\mathcal{D}$  with  $M$  samples.

The calculation of the aggregate cost value is followed by an optimization on the cost function  $J(\theta)$ . The *Gradient Descent* approach is the employed optimization method, where the minimum of the function  $J(\theta)$  is found by taking the partial derivative of this function with respect to the parameter vector  $\theta$  and updating each parameter in  $\theta$  simultaneously based on a learning rate  $\eta$  and the corresponding gradient:

$$\theta_j = \theta_j - \eta \frac{\partial}{\partial \theta_j} J(\theta) \quad (16)$$

The Gradient Descent routine is repetitively run until the parameter vector  $\theta$  converges. On the other hand, the performance of the VQA is monitored through an accuracy metric, which is simply a measure for all of the labels predicted correctly:

$$\text{Accuracy} = \frac{\text{Number of correct predictions}}{\text{Total number of predictions}} \quad (17)$$

## V. EXPERIMENTAL RESULTS

The user localization dataset includes 2000 samples and 4 classes in total. Those classes are associated to 4 different locations in a facility and there are 500 samples for each of the class. Every sample is composed of 7 features related to the signal strengths received from 7 routers and a class label representing the location of the user. In consideration of a binary classification task, 800 samples are extracted from the dataset equally split between Class 1 and Class 2. On the other hand, 75% of the data is used for the training purpose, whereas the proposed learning model is validated with the rest of the data.

The simulations are carried out with PennyLane [28], a Python software framework for differentiable programming of quantum computers. It provides the necessary tools for the construction of gate-based quantum circuits, and in particular of the variational quantum circuit implemented in this work. In addition to the quantum computation based routines, PennyLane makes use of the classical optimization methods executed as a classical part of the hybrid quantum-classical environment.

To evaluate the performance, the proposed QML model is prepared as the VQA depicted in Fig. 3. First, each sample in the dataset is padded with 0 in order to meet the condition of

having 8 amplitudes required for a 3-qubit quantum system. The padded samples are scaled and normalized, which is also mandatory due to the fact that all quantum states have a unit length of 1.

After the sample is mapped to a quantum state with the aid of amplitude encoding scheme, a unitary transformation of the quantum state is performed in the variational quantum circuit. The experimental setup provides 4 variants of the VQA depending on the number of layers varying between the range 4 and 7. Each layer of the quantum circuit includes 3 RY rotation gates and 3 CNOT gates. Expectation values, which are the predictions, and the true labels are passed to the cost function aiming to determine the amount of error for the classification task. Next, a Gradient Descent Optimization takes place to obtain the best parameter values minimizing the cost function value. The updated parameters adjust the amount of qubit rotations in the VQC for the next iteration of the learning process.

The mentioned variational quantum algorithm variants with different number of VQC layers are compared in terms of cost and accuracy at every epoch. In total, there are 10 epochs, each of which includes 12 iterations since the training dataset of 600 samples are processed in batches of 50 samples. The means of cost and accuracy for each epoch are calculated through 12 iterations of the corresponding epoch.

The cost value for the VQA with 4-layered VQC is significantly higher than that of the other VQA variants in the early stages of the epochs for both of training and test datasets (Fig. 4). As the VQC parameters converge, it is obvious that all of the cost values decrease smoothly. It is almost zero in the case of training dataset, whereas cost of testing phase remains in the range between 0.2 – 0.4. Similarly, the outcome for the accuracy metric shows that all of the VQAs achieve a score of almost 100% during the training phase. However, the case differs for predicting the unseen labels such that the accuracy values rise without any fluctuation except for the 4-layered VQC until the range of 84% – 93% is reached. The highest achieved results are summarized in Table 3.

The best accuracy value throughout the test epochs is obtained at Epoch 3 when the 7-layered VQC is utilized. Nevertheless, its accuracy curve drops below the curve of the VQC with 6 layers, which is an indication of overfitting. This fact forces us to follow one of the two precautions to mitigate the overfitting issue: 1) The 7-layered VQC setup has to be stopped at earlier epochs through capturing a possible lower value of the next epoch. 2) Use directly the 6-layered VQC, which has 18 trainable parameters. Note that the VQCs with 4, 5, 6 and 7 layers contain 12, 15, 18 and 21 parameters, respectively.

TABLE III. BEST RESULTS FOR COST AND ACCURACY

VQC Layer Size	Training Dataset			Test Dataset		
	Cost	Accuracy	Epoch	Cost	Accuracy	Epoch
4	0.02889	0.98556	10	0.31417	0.84292	10
5	0.02000	0.99000	10	0.28250	0.85875	10
6	<b>0.01611</b>	<b>0.99194</b>	10	0.18750	0.90625	9
7	0.02167	0.98917	5	<b>0.14417</b>	<b>0.92792</b>	3

With the aim of emphasizing the true potential of variational quantum algorithms, the devised VQA is compared against the well-known machine learning

algorithms such as Naïve Bayes, K-Nearest Neighbor, Logistic Regression and Support Vector Machine. It is observed that the VQCs with 6 and 7 layers perform better than the classical counterparts in terms of testing accuracy (Table 4). In relation to the training performances of compared algorithms, the 6-layered VQC achieves the second best result after the K-Nearest Neighbor algorithm.

TABLE IV. COMPARISON WITH WELL-KNOWN MACHINE LEARNING ALGORITHMS

Algorithms	Training Accuracy	Testing Accuracy
Naïve Bayes	0.99166	0.89500
K-Nearest Neighbor	<b>0.99666</b>	0.90500
Logistic Regression	0.99000	0.86500
Support Vector Machine	0.98666	0.84000
VQC with 6 Layers	<b>0.99194</b>	<b>0.90625</b>
VQC with 7 Layers	0.98917	<b>0.92792</b>

A software simulation environment with a lot of tunable parameters holds the disadvantage of longer execution times. At the same time, increasing the layer size or the depth of a quantum circuit and running it on a real quantum hardware of NISQ era may result in decoherence, which negatively affects the expected outcomes and degrades the performance. The major consequence of the simulation results is that the potential of quantum computing is evident for machine learning tasks. Also, the key component for solving large learning problems is likely to be the QML approaches with the advances in the fault tolerant quantum computers having more qubits than the NISQ devices.

## CONCLUSION

This work presented the design of a variational quantum algorithm consisting of data preprocessing, sample encoding, unitary evolution of quantum states, predictions based on measurement results, cost function optimization and parameter tuning. We especially focused on layered structure of the variational circuit employed in the proposed VQA. One of the foremost findings of this research is that the number of layers is of great importance to attain better results out of the classification task. Secondly, keeping the layer size at a reasonable amount is a key factor to mitigate the overfitting issue.

The implemented algorithm is evaluated with a publicly accessible dataset tackling with the problem of user localization. For detecting the actual locations of users possessing mobile devices, the signal strengths received from several routers are exploited. From the original dataset, we have extracted the samples associated with only two locations to present a two-label classifier scheme. The simulation results demonstrated the efficiency and applicability of quantum machine learning approaches on real world problems. An accuracy rate of 99% was achieved for the prediction of class 1 and class 2 labels during the learning stage. We furtherly observed that the performance of our VQA while evaluating with test samples was around 93% in terms of accuracy.

As a future direction, our research has to be extended to cover the multi-class classification ability on the employed dataset. This particularly requires a design update in the variational quantum circuit part. A further investigation can be maintained on the complex learning tasks with a bigger feature and sample space taking the limitations of near-term NISQ

devices into the consideration. Furthermore, we plan to implement the developed quantum machine learning model on the cloud platforms, on which real quantum computers are accessible for public use.

#### CONTRIBUTION OF THE AUTHORS

The contributions of the authors to the article are equal.

#### CONFLICT OF INTEREST

There is no conflict of interest between the authors.

#### STATEMENT OF RESEARCH AND PUBLICATION ETHICS

Research and publication ethics were observed in this study.

#### REFERENCES

- [1] Michael A. Nielsen and Isaac Chuang, Quantum computation and quantum information. Cambridge, UK: Cambridge University Press, 2002.
- [2] Peter W. Shor, "Algorithms for quantum computation: discrete logarithms and factoring," in *Proc. 35th annual symposium on foundations of computer science*, 1994, pp. 124-134.
- [3] Lov K. Grover, "A fast quantum mechanical algorithm for database search," in *Proc. the twenty-eighth annual ACM symposium on Theory of computing*, 1996, pp. 212-219.
- [4] Seth Lloyd, "Universal quantum simulators," *Science*, vol. 273, no. 5278, pp. 1073-1078, Aug. 23, 1996.
- [5] Robin Harper, Steven T. Flammia, and Joel J. Wallman, "Efficient learning of quantum noise," *Nature Physics*, vol. 16, no. 12, pp. 1184-1188, Dec. 2020.
- [6] John Preskill, "Quantum computing in the NISQ era and beyond," *Quantum*, vol. 2, no. 79, pp. 1-20, Jul. 30, 2018.
- [7] Sukhpal Singh Gill *et al.*, "Quantum computing: A taxonomy, systematic review and future directions," *Software: Practice and Experience*, vol. 52, no. 1, pp. 66-114, Oct. 7, 2022.
- [8] N. Schetakis, D. Aghamalyan, P. Griffin, and M. Boguslavsky, "Review of some existing QML frameworks and novel hybrid classical-quantum neural networks realising binary classification for the noisy datasets," *Scientific Reports*, vol. 12, no. 1, pp. 1-12, Jul. 13, 2022.
- [9] Maria Schuld and Francesco Petruccione, *Machine learning with quantum computers*, Berlin, Germany: Springer, 2021.
- [10] Tariq M. Khan and Antonio Robles-Kelly, "Machine learning: quantum vs classical," *IEEE Access*, vol. 8, pp. 219275-219294, Dec. 1, 2020.
- [11] L. Alchieri, D. Badalotti, P. Bonardi, and S. Bianco, "An introduction to quantum machine learning: from quantum logic to quantum deep learning," *Quantum Machine Intelligence*, vol. 3, pp. 1-30, Nov. 15, 2021.
- [12] S. Y. C. Chen and S. Yoo, "Federated quantum machine learning," *Entropy*, vol. 23, no. 4, pp. 1-15, Apr. 13, 2021.
- [13] Y. Du, T. Huang, S. You, M. H. Hsieh, and D. Tao, "Quantum circuit architecture search: error mitigation and trainability enhancement for variational quantum solvers," 2020, *arXiv:2010.10217*.
- [14] T. Hubregtsen, J. Pichlmeier, P. Stecher, and K. Bertels, "Evaluation of parameterized quantum circuits: on the relation between classification accuracy, expressibility, and entangling capability," *Quantum Machine Intelligence*, vol. 3, pp. 1-19, Mar. 11, 2021.
- [15] Samuel Yen-Chi Chen *et al.*, "Variational quantum circuits for deep reinforcement learning," *IEEE Access*, vol. 8, pp. 141007-141024, Jul. 20, 2020.
- [16] A. Al-Habashna, G. Wainer, and Moayad Aloqaily, "Machine learning-based indoor localization and occupancy estimation using 5G ultra-dense networks," *Simulation Modelling Practice and Theory*, vol. 118, pp. 1-17, 2022.
- [17] P. S. Varma and Veena Anand, "Fault-Tolerant indoor localization based on speed conscious recurrent neural network using Kullback-Leibler divergence," *Peer-to-Peer Networking and Applications*, vol. 15, no. 3, pp. 1370-1384, Feb. 25, 2022.
- [18] K. Ngamakeur, S. Yongchareon, J. Yu, and S. Islam, "Passive infrared sensor dataset and deep learning models for device-free indoor localization and tracking," *Pervasive and Mobile Computing*, vol. 88, pp. 1-16, 2023.
- [19] J. Xue, J. Liu, M. Sheng, Y. Shi, and J. Li, "A WiFi fingerprint based high-adaptability indoor localization via machine learning," *China Communications*, vol. 17, no. 7, pp. 247-259, Jul. 24, 2020.

# Wireless Communication Between Vehicles: Exploring the Potential of V2V and V2X Communication for Improved Efficiency, Safety, and Sustainability

Received 16 June 2023; Accepted: 29 June 2023

Research Article

Mohammed Alsudani  
Electrical and Electronic Engineering  
karabuk university  
Karabuk, Turkey  
mode8427@gmail.com  
0000-0000-0000-0000

**Abstract—** Vehicle-to-Vehicle (V2V) communication is a groundbreaking technology that promises to reshape transportation systems globally. This paper delves into the diverse applications of V2V communication, emphasizing its potential to enhance traffic efficiency, road safety, and environmental sustainability. By facilitating real-time information exchange between vehicles, V2V communication can aid in collision prevention, traffic flow optimization, and emission reduction, thereby fostering a more secure, efficient, and eco-friendly transportation landscape. The analysis presented in this paper encompasses the key components and benefits of V2V communication, along with an exploration of its far-reaching implications for the future of transportation, including the advancement of autonomous vehicles and the establishment of greener, more sustainable transport networks.

**Keywords—** Vehicle-to-Vehicle communication, V2V, traffic efficiency, road safety, traffic flow optimization, autonomous vehicles, sustainable transportation.

## I. INTRODUCTION

With the rapid growth of smart cities and the Internet of Things (IoT), connectivity has become an essential aspect of modern life. This connectivity extends to the transportation industry, where wireless communication between vehicles is poised to play a vital role in enhancing road safety, optimizing traffic flow, and facilitating the development of autonomous vehicles. This paper provides an overview of the various technologies and applications related to wireless communication between vehicles, addressing both the opportunities and the challenges that lie ahead. [1]

In recent years, the transportation industry has been undergoing a significant transformation, fueled by advancements in communication and information technologies. The growing importance of connectivity in everyday life, combined with the rise of smart cities and the Internet of Things (IoT), has led to an increased focus on enabling wireless communication between vehicles. This enhanced connectivity is expected to bring about a paradigm shift in the way we approach transportation, with implications for road safety, traffic management, and the development of autonomous vehicles. This paper aims to provide an in-depth examination of the technologies,

benefits, and challenges associated with wireless communication between vehicles and the methodologies that can be employed to study these topics.[2]

Moreover, V2V communication, or Vehicle-to-Vehicle communication, refers to the exchange of information between vehicles through wireless networks. This technology allows vehicles to share critical data, such as their position, speed, and direction, with nearby vehicles in real-time. V2V communication is a crucial component of connected vehicle systems and plays a significant role in improving road safety, reducing traffic congestion, and supporting the development of autonomous vehicles.

By enabling vehicles to communicate with each other, V2V communication helps drivers or autonomous systems anticipate potential hazards and adjust their actions accordingly. For instance, if a car ahead suddenly brakes, the following vehicles can receive this information and react promptly, minimizing the risk of collisions.

Overall, V2V communication is a vital component of the future of transportation, paving the way for safer, more efficient, and intelligent roadways.[3]

## II. TECHNOLOGIES ENABLING WIRELESS COMMUNICATION BETWEEN VEHICLES

Several wireless communication technologies enable the exchange of information between vehicles in V2V communication systems. These technologies provide real-time, low-latency communication, which is essential for ensuring the safety and efficiency of connected vehicles. Here are some of the key technologies enabling wireless communication between vehicles:

### A. Dedicated Short-Range Communications (DSRC)

DSRC is a radio communication technology operating in the 5.9 GHz frequency band. It is specifically designed for V2V and Vehicle-to-Infrastructure (V2I) communication, providing low-latency, short-range communication that is well-suited for safety-critical applications.[4] As shown the (DSRC) in the figure 1.



Fig. 1. The Dedicated Short-Range Communications

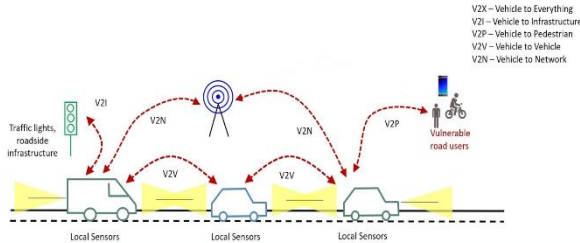


Fig. 2. The Cellular Vehicle-to-Everything



Fig. 2. The 5G New Radio (NR)

### B. Cellular Vehicle-to-Everything (C-V2X)

C-V2X technology leverages existing cellular networks (e.g., 4G LTE, 5G) to facilitate communication between vehicles, infrastructure, and other road users. C-V2X offers longer communication ranges and enhanced reliability compared to DSRC, making it suitable for various V2V and V2I applications. [5] As shown the (C-V2X) in figure 2.

### C. 5G New Radio (NR)

The 5G NR technology offers ultra-reliable, low-latency communication, which is critical for V2V applications. With its high data rates and capacity, 5G NR enables advanced applications, such as autonomous driving and high-definition map updates, and supports the massive amounts of data exchanged in V2X communication.[6] As shown the 5G New Radio (NR) in figure 3.

### D. Wi-Fi (802.11p)

Wi-Fi-based V2V communication uses the 802.11p standard, which is an amendment to the IEEE 802.11 standard for wireless local area networks (WLANs). It has been specifically designed for automotive environments, providing fast and reliable communication for V2V and V2I applications [7] As shown the Wi-Fi (802.11p) in figure 4.

## III. HOW DOES V2V COMMUNICATION WORK

Vehicle-to-Vehicle (V2V) communication works by enabling vehicles to exchange information with each other over wireless networks, typically using Dedicated Short-Range Communications (DSRC)/Cellular Vehicle-to-

Everything (C-V2X) technology/C.5G New Radio (NR) or wi-fi (802.11p)

Here is a step-by-step explanation of how V2V communication works:

### A. Data Collection

Each vehicle collects data from its onboard sensors, such as GPS, radar, LiDAR, and cameras, which provide information on the vehicle's position, speed, direction, and other dynamic attributes.

### B. Data Processing

The vehicle's onboard computer processes this data to generate relevant information, such as potential hazards, traffic updates, or weather conditions. This information is then prepared for transmission to other nearby vehicles.

### C. Wireless Transmission

The processed information is broadcasted using wireless communication technology. DSRC operates in the 5.9 GHz frequency band, whereas C-V2X uses cellular networks like LTE or 5G. These technologies provide low-latency, high-reliability communication channels that enable vehicles to communicate over short to medium distances (typically up to 1000 meters)

### D. Data Reception

Nearby vehicles receive the broadcasted information through their onboard communication systems. The received data is integrated with the vehicle's existing sensor data to provide a more comprehensive understanding of the surrounding environment.

### E. Decision-Making

Based on the received information, the vehicle's onboard computer, Advanced Driver Assistance Systems (ADAS), or autonomous driving systems can make informed decisions to adjust vehicle behavior, such as slowing down, changing lanes, or taking evasive action in response to potential hazards.

### F. Action Execution

The vehicle's control systems implement the decisions made by the onboard computer or ADAS, adjusting the vehicle's speed, direction, or other parameters to ensure safe and efficient navigation. In summary, V2V communication works by collecting, processing, and transmitting data between vehicles over wireless networks, allowing them to share critical information in real-time. This exchange of information helps drivers or autonomous systems make informed decisions, improving road safety, reducing traffic congestion, and supporting the development of autonomous vehicles.[8, 9]

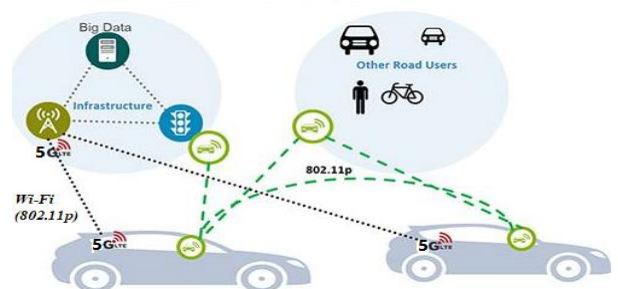


Fig. 4. The Wi-Fi (802.11p)

#### IV. COMPONENTS AND APPLICATIONS OF V2V COMMUNICATION

##### A. Components of V2V Communication

The components of Vehicle-to-Vehicle (V2V) communication play a crucial role in enabling vehicles to exchange information wirelessly. The primary components involved in V2V communication include in the table 1 :Applications of V2V Communication

Vehicle-to-Vehicle (V2V) communication refers to the exchange of information between vehicles using wireless communication technologies. It has gained significant attention in recent years due to its potential to improve road safety, traffic efficiency, and environmental sustainability. Here are some key applications of V2V communication:

- 1) *Traffic Congestion Management:* By sharing traffic-related information, vehicles can optimize their routes and avoid congested areas, leading to better traffic flow and reduced travel time.
- 2) *Cooperative Adaptive Cruise Control (CACC):* V2V communication enables vehicles to maintain a safe distance from each other while driving at a constant speed, reducing the likelihood of traffic jams and improving overall traffic efficiency.
- 3) *Platooning:* V2V communication can be used to form platoons of vehicles driving in close proximity, which can lead to improved fuel efficiency, reduced emissions, and increased road capacity.
- 4) *Autonomous Vehicle Integration:* V2V communication plays a crucial role in the development and deployment of autonomous vehicles by providing essential information about the surrounding environment and enabling cooperative behavior among vehicles.

These applications of V2V communication hold the promise of revolutionizing the transportation sector by significantly enhancing road safety, reducing traffic congestion, and contributing to a greener environment.[9, 11, 12]

#### V. IMPACTS OF V2V COMMUNICATION

The impacts of V2V communication on traffic efficiency, road safety, and the environment can be significant, providing a range of benefits that can enhance the transportation sector's sustainability and efficiency. As the technology continues to evolve and become more widespread, we can expect to see further improvements in these areas, leading to safer, more efficient, and sustainable transportation solutions. Here we can explain some the impacts of V2V communication.

##### A. Traffic Efficiency

V2V communication has the potential to significantly enhance traffic efficiency through various means. By enabling vehicles to exchange real-time information with each other, V2V technology can lead to better traffic management, reduced congestion, and optimized travel routes. Here are some of the ways V2V communication impacts traffic efficiency:

- 1) *Real-time Traffic Updates :* V2V communication allows vehicles to share real-time traffic data, enabling drivers to make informed decisions about their routes, avoiding congestion, and reducing travel times.

- 2) *Traffic Signal Adjustments:* V2V communication can provide information about traffic conditions to traffic management systems, allowing them to optimize signal timings and improve traffic flow.
- 3) *Reduced Traffic Congestion:* By facilitating cooperation among vehicles and sharing traffic information, V2V communication helps in reducing traffic congestion and improving overall road efficiency.
- 4) *Improved Fuel Efficiency :* V2V communication enables more efficient driving patterns, such as cooperative adaptive cruise control, which can result in reduced fuel consumption and lower emissions.[9, 13]

##### B. Road Safety

V2V communication has a significant impact on road safety by allowing vehicles to share real-time information about their positions, speeds, and trajectories with each other. This enhanced situational awareness can help prevent accidents, reduce the severity of crashes, and save lives. Here are five ways V2V communication contributes to road safety:

- 1) *Collision Avoidance:* V2V communication enables vehicles to predict and avoid potential collisions by sharing data about their positions, speeds, and trajectories with nearby vehicles. This can help reduce the number of accidents and minimize the severity of crashes when they occur.
- 2) *Intersection Safety:* V2V communication can improve safety at intersections by allowing vehicles to share information about their intentions to turn, change lanes, or pass through the intersection. This helps prevent crashes resulting from miscommunication or lack of visibility, especially in complex or congested intersections.
- 3) *Emergency Vehicle Notification:* V2V communication can alert nearby vehicles to the presence of emergency vehicles, such as ambulances, fire trucks, or police cars. This enables drivers to take appropriate actions to clear a path, ensuring faster and safer emergency response.

TABLE V. COMPONENTS OF V2V COMMUNICATION

Component	Description
1. Onboard Sensors	Collect data on position, speed, direction, etc., from GPS, radar, LiDAR, and cameras.
2. Onboard Computer	Process sensor data, generate information for transmission, and make decisions.
3.V2V Communication Module	Transmit and receive data using DSRC or C-V2X technologies.
4. Antenna	Transmit and receive wireless signals, ensuring reliable connections within range.
5. User Interface	Display V2V information to the driver through infotainment, dashboard, or dedicated devices.
6. Control Systems	Implement decisions made by onboard computer or ADAS for safe and efficient navigation.

*Note: Security mechanisms like encryption, authentication, and message signing are essential for maintaining secure and private communication between vehicles.[9, 10]*

4) *Vulnerable Road User Protection:* By integrating V2V communication with other technologies, such as Vehicle-to-Pedestrian (V2P) or Vehicle-to-Bicycle (V2B) communication, the safety of vulnerable road users, like pedestrians and cyclists, can be enhanced. This can help prevent accidents involving these road users, who are often more susceptible to serious injuries or fatalities.

5) *Enhanced Driving Assistance Systems:* V2V communication can augment Advanced Driver Assistance Systems (ADAS) by providing additional information from surrounding vehicles, enabling more accurate decision-making and improved safety features, such as blind-spot monitoring, lane-keeping assistance, and automatic emergency braking.[14, 15]

### C. Environment

V2V communication has the potential to positively impact the environment by promoting more efficient driving behavior, reducing traffic congestion, and supporting the integration of eco-friendly technologies. Here are some ways in which V2V communication can contribute to a greener environment:

1) *Eco-routing:* V2V communication enables vehicles to share real-time traffic information, allowing them to optimize their routes based on traffic conditions and minimize fuel consumption. By reducing the time spent idling in traffic, vehicles can emit fewer greenhouse gases and pollutants.

2) *Fuel-efficient driving:* V2V communication can facilitate cooperative driving behaviors, such as platooning and Cooperative Adaptive Cruise Control (CACC), which help maintain constant speeds and minimize sudden braking or acceleration. These behaviors lead to more efficient fuel consumption and reduced emissions.

3) *Reduced traffic congestion:* By enhancing traffic flow and reducing congestion through improved route planning and traffic management, V2V communication can contribute to lower overall fuel consumption and emissions, as vehicles spend less time idling or moving at inefficient speeds.

4) *Support for electric vehicles (EVs):* V2V communication can help improve EV infrastructure by sharing information about charging station locations, availability, and charging times, encouraging EV adoption and reducing dependence on fossil fuels.

5) *Integration of renewable energy:* V2V communication can support the integration of renewable energy sources into the transportation sector by enabling vehicles to communicate with smart grids and optimize energy consumption based on the availability of renewable energy.

6) *Smarter urban planning:* Data collected through V2V communication can be used by city planners and transportation authorities to identify areas with high traffic congestion or poor air quality, enabling the development of

more sustainable and environmentally friendly urban designs.[16]

## VI. CHALLENGES AND FUTURE PROSPECTS

### A. Challenges

Despite the numerous benefits and applications of V2V communication, several challenges must be addressed to realize its full potential. Here are some key challenges and future prospects in the field of V2V communication.

1) *Security and Privacy:* Ensuring secure and private communication between vehicles is crucial to prevent cyberattacks, data breaches, and unauthorized access. Developing robust security protocols, encryption methods, and authentication techniques will be essential for safeguarding V2V communication systems.

2) *Interoperability:* As multiple wireless communication technologies exist for V2V communication, ensuring seamless interoperability between different vehicles and infrastructure systems is vital. Establishing common communication standards and protocols will help achieve better integration and coordination among various V2X technologies.

3) *Scalability:* As the number of connected vehicles increases, V2V communication systems must be able to scale efficiently to handle the massive amounts of data exchanged between vehicles. Advances in network infrastructure, data management, and edge computing will be crucial to ensure the scalability of V2V communication systems.

4) *Spectrum Allocation:* With the increasing demand for wireless communication technologies, competition for available radio spectrum is intensifying. Efficient spectrum allocation and management will be necessary to avoid interference and ensure the reliable performance of V2V communication systems.

5) *Legal and Regulatory Frameworks:* The development of comprehensive legal and regulatory frameworks is essential for the widespread adoption of V2V communication. These frameworks should address issues such as liability, data ownership, and privacy while facilitating the integration of V2V technologies into existing transportation systems.

6) *Public Acceptance:* Gaining public trust and acceptance of V2V communication technologies is vital for their successful implementation. Public awareness campaigns, education, and transparency about the benefits and potential risks associated with V2V communication will be crucial in building public confidence. [17-20]

### B. Future Prospects

As these challenges are addressed, the future of V2V communication holds significant promise. The development of advanced communication technologies, such as 5G and 6G, will further enhance the capabilities of V2V systems, enabling new applications like fully autonomous driving and smart city integration. Additionally, the increasing adoption of electric and hybrid vehicles will drive the demand for advanced V2V

communication systems to optimize energy consumption, route planning, and charging infrastructure.

### CONCLUSION

In conclusion, V2V communication offers immense potential to transform the transportation landscape by facilitating real-time information exchange between vehicles, resulting in improved road safety, traffic efficiency, and environmental sustainability. The development and integration of wireless communication technologies, such as DSRC, C-V2X, and 5G NR, have enabled a wide range of V2V applications, from collision avoidance to autonomous vehicle integration. However, challenges such as security and privacy, interoperability, and regulatory frameworks must be addressed to fully realize the potential of V2V communication. As the technology continues to advance and overcome these challenges, V2V communication is expected to become a key enabler of intelligent transportation systems and autonomous driving, ultimately leading to safer, more efficient, and greener transportation solutions for future generations.

### CONTRIBUTION OF THE AUTHORS

The contributions of the authors to the article are equal.

### CONFLICT OF INTEREST

There is no conflict of interest between the authors.

### STATEMENT OF RESEARCH AND PUBLICATION ETHICS

Research and publication ethics were observed in this study

### REFERENCES

- [1] A. Rejeb, K. Rejeb, S. Simske, H. Treiblmaier, and S. Zailani, "The big picture on the internet of things and the smart city: a review of what we know and what we need to know," *Internet of Things*, vol. 19, p. 100565, 2022.
- [2] K. Jones, "How the internet of things is building smarter cities," in *World Economic Forum in a cooperation with Visual Capitalist*. Retrieved April, 2020, vol. 10, p. 2020.
- [3] E. Smith, "The Future of Intelligent Transportation Systems (ITS): Applying Lessons Learned From 30 Years of Innovation," *Public Roads*, vol. 86, no. 1, 2022.
- [4] J. B. Kenney, "Dedicated short-range communications (DSRC) standards in the United States," *Proceedings of the IEEE*, vol. 99, no. 7, pp. 1162-1182, 2011.
- [5] S. Chen *et al.*, *Cellular Vehicle-to-Everything (C-V2X)*. Springer Nature, 2023.
- [6] K. Serizawa, M. Mikami, K. Moto, and H. Yoshino, "Field trial activities on 5G NR V2V direct communication towards application to truck platooning," in *2019 IEEE 90th Vehicular Technology Conference (VTC2019-Fall)*, 2019, pp. 1-5: IEEE.
- [7] G. Cecchini, A. Bazzi, B. M. Masini, and A. Zanella, "Performance comparison between IEEE 802.11 p and LTE-V2V in-coverage and out-of-coverage for cooperative awareness," in *2017 IEEE Vehicular Networking Conference (VNC)*, 2017, pp. 109-114: IEEE.
- [8] J. Harding *et al.*, "Vehicle-to-vehicle communications: readiness of V2V technology for application," United States. National Highway Traffic Safety Administration 2014.
- [9] M. El Zorkany, A. Yasser, and A. I. Galal, "Vehicle to vehicle "V2V" communication: scope, importance, challenges, research directions and future," *The Open Transportation Journal*, vol. 14, no. 1, 2020.
- [10] A. Demba and D. P. Möller, "Vehicle-to-vehicle communication technology," in *2018 IEEE international conference on electro/information technology (EIT)*, 2018, pp. 0459-0464: IEEE.
- [11] J. E. Siegel, D. C. Erb, and S. E. Sarma, "A survey of the connected vehicle landscape—Architectures, enabling technologies, applications, and development areas," *IEEE Transactions on Intelligent Transportation Systems*, vol. 19, no. 8, pp. 2391-2406, 2017.
- [12] A. Muza, S. Kamarulzaman, M. Rahman, S. Murad, M. Kamal, and A. Alenezi, "Multiple Vehicle Cooperation and Collision Avoidance in Automated Vehicles: Survey and an AI-Enabled Conceptual Framework," 2022.
- [13] S. Wong, L. Jiang, R. Walters, T. G. Molnár, G. Orosz, and R. Yu, "Traffic forecasting using vehicle-to-vehicle communication," in *Learning for Dynamics and Control*, 2021, pp. 917-929: PMLR.
- [14] A. Metzner and T. Wickramaratne, "Exploiting Vehicle-to-Vehicle Communications for Enhanced Situational Awareness," in *2019 IEEE Conference on Cognitive and Computational Aspects of Situation Management (CogSIMA)*, 2019, pp. 88-92: IEEE.
- [15] M. Mostaed, K. Aldabas, and C. Olaverri-Monreal, "V2V Communication System to Increase Driver Awareness of Emergency Vehicles," in *Computer Aided Systems Theory—EUROCAST 2017: 16th International Conference, Las Palmas de Gran Canaria, Spain, February 19-24, 2017, Revised Selected Papers, Part II 16*, 2018, pp. 413-418: Springer.
- [16] F. I. Rahman, "Impact of V2V Communication on Eco-Route Choice," *LOGI-Scientific Journal on Transport and Logistics*, vol. 11, no. 1, pp. 37-45, 2020.
- [17] M. A. Habib *et al.*, "Security and privacy based access control model for internet of connected vehicles," *Future Generation Computer Systems*, vol. 97, pp. 687-696, 2019.
- [18] L. Jin and P. Slowik, "Literature review of electric vehicle consumer awareness and outreach activities," *International Council on Clean Transportation*. Available from internet: [https://www.theicct.org/sites/default/files/publications/Consumer-EV-Awareness\\_ICCT\\_Working-Paper\\_23032017\\_vF.pdf](https://www.theicct.org/sites/default/files/publications/Consumer-EV-Awareness_ICCT_Working-Paper_23032017_vF.pdf), 2017.
- [19] L. C. Ezenwa, "Wireless V2V Communication with DSRC Technology in Comparison to C-V2X," *ATZ worldwide*, vol. 124, no. 6, pp. 40-43, 2022.
- [20] P. Wang, W. Wu, J. Liu, G. Chai, and L. Feng, "Joint Spectrum and Power Allocation for V2X Communications with Imperfect CSI," *arXiv preprint arXiv:2302.14704*, 2023.

# Maximum Power Point Tracking Achievements and Challenges in Photovoltaic Systems: Review

Received: 28 May 2023 ; Revised: 15 June 2023

Accepted: 25 June 2023

Review Article

Ahmed Mousay  
Department of electrical engineering  
University of Karabuk  
Karabuk, Turkey  
ahmedmohammedmousay@gmail.com  
0009-0007-6588-845X

**Abstract**— The ever-increasing demand for electrical energy in recent decades has necessitated the exploration of alternative energy sources, one of which is solar energy. The most practical means of utilizing solar energy is through the use of a Photovoltaic (PV) system. Nevertheless, the energy harvested by PV modules is constrained by low conversion efficiency, nonlinearity, and susceptibility to weather conditions, such as temperature and irradiance levels. To address these limitations, Maximum Power Point Tracking (MPPT) techniques have been developed to optimize the output of PV systems under specific circumstances. This academic article provides an in-depth analysis of the most widely used MPPT techniques, utilizing both traditional and soft computing methods. The article discusses the fundamental principles and practical applications of these techniques, as well as the challenges associated with MPPT, such as coping with rapidly changing irradiance and partial shading scenarios.

**Keywords**—maximum power point tracking (MPPT); Photovoltaic (PV); partial shading; fast irradiance.

## I. INTRODUCTION

In recent decades, there has been a significant increase for electricity demand, driven by factors such as population growth, modern lifestyle demands, and the acceleration of the industrial revolution. This surge in demand has been accompanied by a rapid rise in the consumption of fossil fuels, which has raised concerns about resource depletion and environmental pollution. Furthermore, the issue of oil scarcity has been further compounded by global climate change [1]. In response to these challenges, researchers and global communities alike have been exploring alternative sources of energy. Solar energy has emerged as a promising option to supplement other renewable energy sources like wind, rain, tides, waves, and geothermal heat, thereby reducing our reliance on fossil fuels. Solar energy offers a host of benefits, including its cleanliness, sustainability, and suitability as an energy source. By mitigating environmental impact and global warming that caused by the utilizing fossil fuels, the adoption of clean energy sources like solar energy can help to reduce CO<sub>2</sub> emissions and promote a healthier planet [2].

Photovoltaic technology is one of the best ways to benefit from solar energy and convert sunlight to electrical energy by using solar cells which is called the PV effect. The name photovoltaic comes from the process of converting sunlight (photons) directly into electricity (voltage). In recent times, many countries have adopted the use of photovoltaic systems in various sectors as a convenient solution to meet their electricity demands. However, these systems have limited efficiency and entail high initial installation costs. To address

these issues, considerable efforts are being made to enhance photovoltaic technology, with the aim of increasing efficiency and reducing costs. Some improvements had developed by scientists such as installation controllers and sensors for the PV system to track the sun continuously and orient a solar panel with the movement of the sun for concentrating the light on the solar cell. However, photovoltaic systems as known still have two problems: the first problem is the low efficiency of energy conversion the PV module. The second problem is the amount of energy which is converted from photons to voltaic by solar cell changes depending on weather conditions like varying temperatures and irradiance amount [3]. The study shows that solar panel converts 35-45% of energy falling into electrical energy, and thus it becomes necessary to use another technique to succeed in dealing with the cost problem and low efficiency of the photovoltaic system[4].

The photovoltaic module's I-V and P-V output power curves are non-linear and have a single point of maximum value called maximum power point (MPP) curve. To achieve optimal efficiency, scientists and researchers have developed a solution to keep tracking the MPP and establish operate point of the photovoltaic (PV) system. However, tracking the MPP can be difficult due to weather variations and changes in loads. There are two categories of techniques proposed to effectively track the MPP in PV system modelling. The first category is based on conventional approaches, such as the fractional open circuit method [5], the short circuit current method [6]. Perturbative & observe method [7], and incremental conductance method [8]. The conventional techniques are easy to implement, cheap and most widely used in commercial products. The second category is based on the soft computing approach, for instance the fuzzy logic control technique [9], the artificial neural network method [10], particle swarm optimization method [11], ant-colony optimization method [12] and differential evolution method [13]. Soft computing techniques are complex structures but have more efficient and fast response better than conventional techniques. However, partial shading and fast-changing irradiance conditions still challenge facing maximum power point tracking techniques. There are numerous academic publications regarding MPPT, making it difficult to keep track of their differences and implementation. According to the literature, there are approximately 40 different techniques for tracking MPP. Some techniques are similar in their operating principles. This paper focuses on the latest and most commonly used techniques for MPPT and addresses the challenges of partial shading and rapidly changing irradiance, which present difficulties for MPPT techniques in photovoltaic systems [14].

## II. CONCEPT OF MPPT

The photovoltaic module's output characteristics exhibit nonlinearity in both I-V and P-V curves, which means that the maximum power output corresponds to a single point at the knee of the curve where current and voltage reach their maximum values. However, the changing of temperature and irradiance levels can influence this point. Figure 1 and Figure 2 demonstrate the I-V and P-V curves under uniform and varied irradiance, respectively. To ensure maximum efficiency, it's necessary to keep track of the varying maximum power points and establish the corresponding MPP to the operating point of the PV system. This is achieved through a process called the maximum power point tracking, which is performed by the use of an electronic subsystem known as the maximum power point tracker (MPPT) system.

The MPPT controller is typically situated between the load and the photovoltaic module, as shown in Figure 3. Its function is to monitor both voltage and current of the PV module and extract the maximum value under specific conditions, as well as to match the photovoltaic system with the load. The MPPT subsystem's sole purpose is to identify the location of the maximum point. Afterwards, a DC-DC converter takes a DC input from the photovoltaic module and converts the current and voltage to AC. It then converts them back to DC, which matches the load based on the MPP to maintain the photovoltaic system's maximum efficiency. To date, photovoltaic efficiency depends on PV module, converter/inverter and MPPT technique efficiencies. Not easily improving the PV module and converter/inverter, because they depend on the available hardware, at variance the MPPT techniques, easy to improve them. Furthermore, several MPPT techniques have been reported in different works. A comparison among many different MPPT techniques has been presented in [15].

## III. CONVENTIONAL MPPT TECHNIQUES

### A. Fractional open circuit voltage technique (FOCVT).

The FOCVT is a simple and efficient approach for tracking the MPP, as it requires minimal parameter input and is easy to implement. This methodology is based on the concept of the highest power point output that can be located by maintaining the PV module's operating voltage ( $V_{pv}$ ) within a range of 72% to 78% of the opening circuit voltage ( $V_{oc}$ ) under consistent conditions of weather [16]. The technique involves regulating the corresponding operating voltage of the PV cell to match a reference voltage ( $V_{ref}$ ) to keep the operating power point run close to MPP, although it may not always be exactly at MPP. The voltage reference is determined using Equation (1).

$$V_{ref} = (0.72 - 0.78) \times V_{oc} \quad (1)$$

The PV module is temporarily isolated from the load and the  $V_{oc}$  is measured, after that the reference voltage  $V_{ref}$  is determined from Eq. (1), and then the converter duty cycle is regulated to make the reference voltage of the PV module equal to the operating voltage, in order to obtain the operating point close to the maximum power point. This technique is easy to implement but the accuracy is low given the periodical shutdown of the converter to measure  $V_{oc}$ .

This algorithm is employed for tracking MPP, as illustrated in Figure 4. This approach disregards the effects of temperature and irradiance.

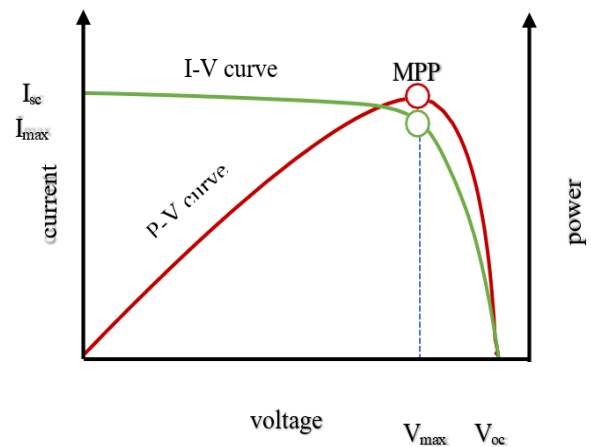


Fig. 1. I-V and P-V curves of PV module under uniform irradiance.

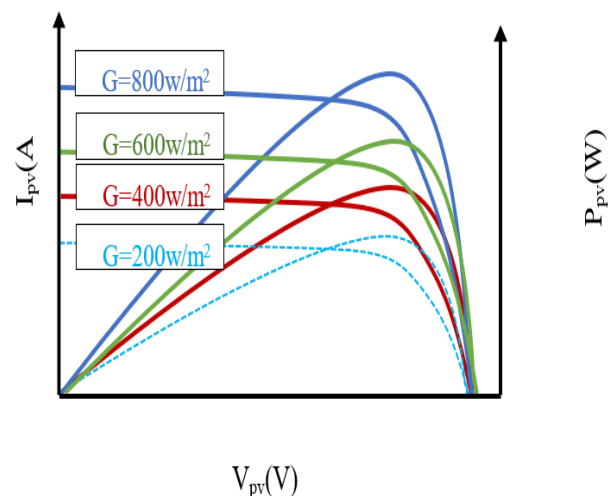


Fig. 2. I-V and P-V curves under various irradiance.

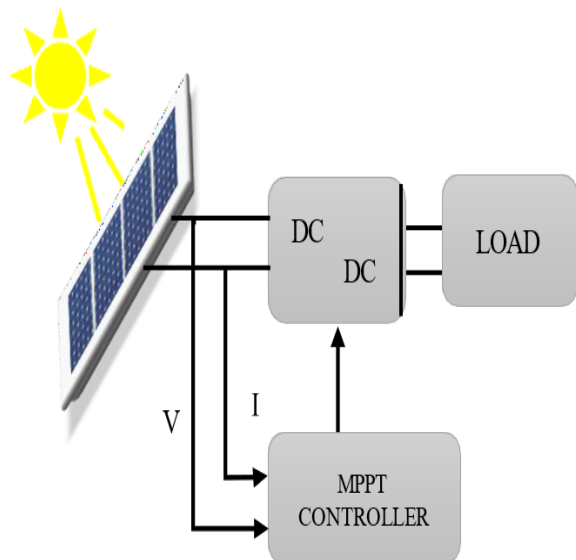


Fig. 3. Structure of photovoltaic system with MPPT controller.

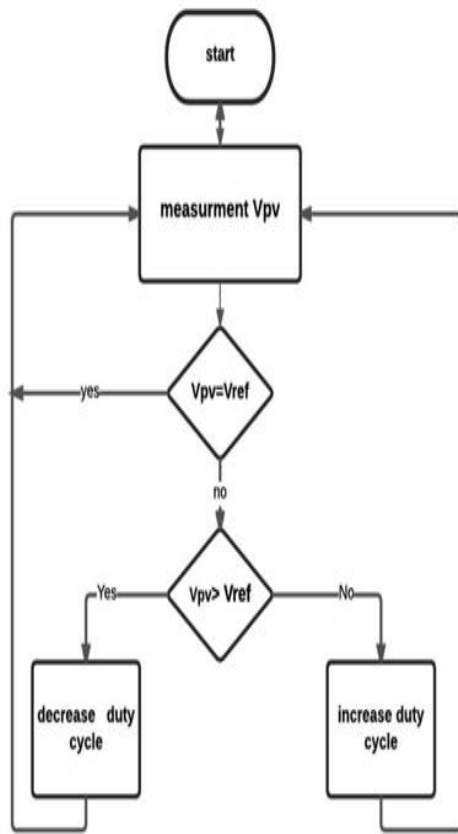


Fig. 4. Flowchart of FOCVT algorithm.

### B. The Fractional short circuit current method.

This method is an alternative approach to tracking the MPP, which is comparable with the fractional open circuit voltage process. However, the key difference is that fractional short circuit current technique operates at a fixed current, while fractional open circuit voltage technique runs at a constant voltage. Identifying the MPP involves detecting the operational current of the PV module within the range of 78% to 92% of the short-circuit current  $I_{sc}$ . In order to maintain the PV system's operational point near the MPP, it is crucial to set and regulate the operational current of the PV module to the reference current  $I_{ref}$  as determined by Equation (2).

$$I_{ref} = (0.78 - 0.92) \times I_{sc} \quad (2)$$

Firstly, we measure the short current  $I_{sc}$ , and afterwards the reference current ( $I_{ref}$ ) is then calculated. After this, the duty cycle of the converter is then adjusted to ensure that operational current  $I_{pv}$  is equivalent to the reference current  $I_{ref}$ . By following this procedure, the operational point of the PV system remains in the vicinity of the MPP. This process is repeated at regular intervals to track the MPP.

### C. The Perturb & Observe (P&O) method.

This technique is a widely known technique used for tracking maximum power point in a photovoltaic (PV) system. The P&O method involves making small changes to the operating point of the system by perturbing both voltage and current in a certain direction, using a constant-sized perturbation. The control algorithm then compares the power value before and after the perturbation. If the power value

increases, it indicates that the operating power is moving towards the MPP. In such cases, these algorithms continue to perturb in the equivalent direction and by the same step size. However, if output power value after perturbation reduces, this denotes that the operating point is stepping away from the MPP, and algorithm governs the reverse perturbation direction with the identical step size. This process is repeated continuously to track the MPP. This procedure is repeated periodically until any changes occur in the weather. Figure 5 illustrates a flowchart of the P&O technique. There are two ways to implement the perturbation, are perturbation based on the direct duty cycle and perturbation based on the reference current/voltage[17]. Equation (3) is the general Equation of the perturbing & observed method.

$$x(k+1)Tp + \text{Sign}(P(K) - P(K-1))Tp \quad (3)$$

where  $x$  is the variable being perturbed either duty cycle or reference current or voltage,  $T_p$  is a period of perturbation,  $dx$  is the amplitude of perturbation and  $P_{pv}$  is the output power of the PV module.

One drawback of the perturb and observe technique is that the module voltage/current is perturbed in every cycle of MPPT, even when the MPP is reached. As a result, the oscillation of the operating point around the ideal MPP persists, causing power loss in the PV system. Figure 6 illustrates the swinging operating point around the MPP. In addition, the P&O technique suffers from misjudgment to track maximum power point fast-changing irradiance condition because the output curve of the PV module is not only a single curve, but some other curves depend on changing irradiance. This means that there are several MPPs, for each curve is one MPP[18].

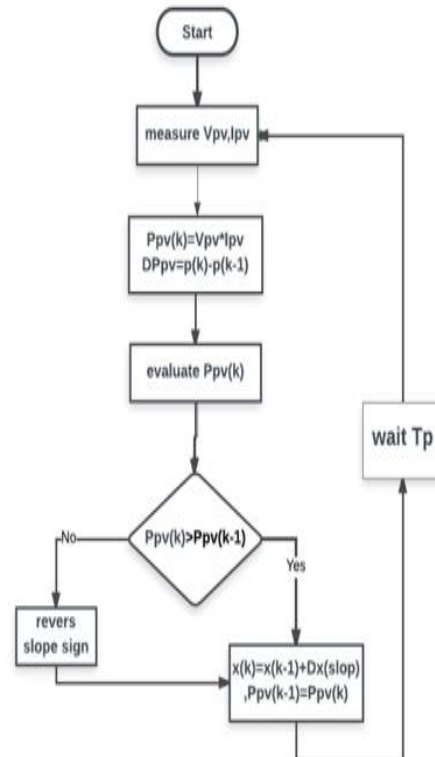


Fig. 5. Flowchart of P&amp;O techniques.

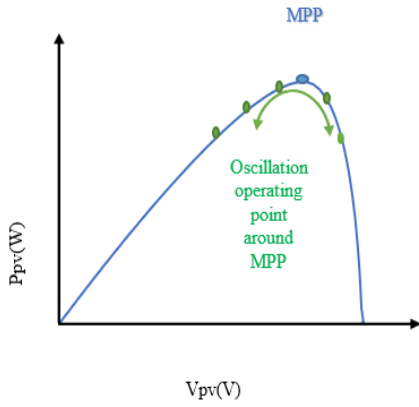


Fig. 6. Oscillation operating point during P&amp;O operation.

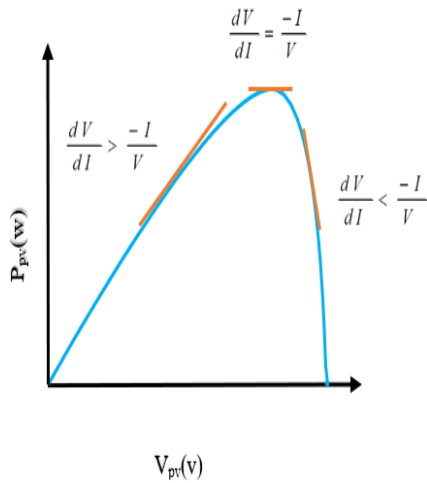


Fig. 7. P-V curve characteristic of Incremental conductance.

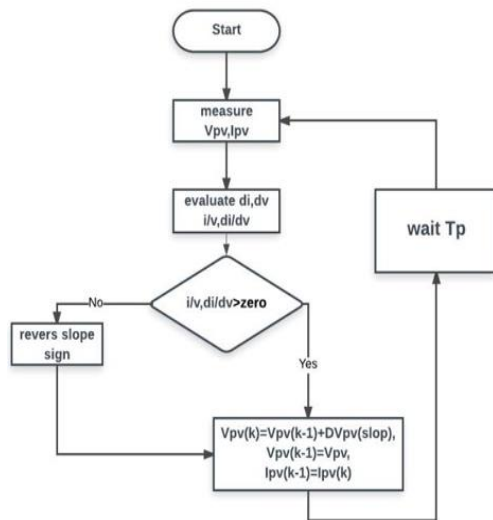


Fig. 8. flowchart of Incremental conductance method.

#### D. Incremental conductance technique.

This technique is another significant method used to determine photovoltaic PV system operating point in relation to the MPP. This technique was developed to address the limitation of the perturb and observe (P&O) technique. This incremental conductance technique relies on the principle that

the MPP is reached when the derivative of the power equation with respect to voltage Eq.(4) equals zero.

$$\frac{dP}{dV} = \frac{d(I \times V)}{dV} = 0 \quad (4)$$

Equation (4) can be expressed as the following Equation.

$$\frac{dI}{dV} = -\frac{I}{V} \quad (5)$$

Based on the fact of Eq. (5), algorithm control compares incremental conductance value  $dI/dV$  with conductance value  $I/V$  with, to know the location of operating point. The incremental conductance technique involves determining the location of maximum power point (MPP) constructed on whether the incremental conductance value is equal to, greater than, or less than the minus conductance value. When the incremental conductance value is equivalent to the negative conductance value, the operating point is at the MPP. If the incremental conductance value surpasses the negative conductance value, then the operational point is positioned to the right of the MPP, and if the incremental conductance value is less than the minus conductance value, the operating point is to the left of the MPP [19]. Figure 7 shows the characteristics of the P-V curve for the incremental conductance technique. Comparable to P&O technique, algorithm control applies perturbation using either a duty ratio perturbation or a feedback voltage perturbation and monitors the relationship between the conductance and incremental conductance. Based on this observation, the control decides whether to either increase or decrease perturbation, as well as to determine the next perturbation's direction, it can either be in the same direction or reversed direction, until the MPP is reached. Then, the control stops the perturbation and the PV system remains operating at the MPP till a change in irradiance changes the location of the MPP. In such a case, the perturbation and observation process is resumed to determine whether the operating point is left or right of the MPP, and the control perturbs again to find a new MPP. This process of adjusting the perturbation and its direction is repeated until the operational point aligns with the MPP once more. Figure 8. shows a flowchart of the incremental conductance method. Equation (6) is repeated to sense a condition in Eq.(5).

$$x(k+1)Tp = x(k)Tp = \text{sign}\left(\frac{I}{V}\right) + \left(\frac{dI}{dV}\right)x \, dx \quad (6)$$

where  $x$  is the perturbed variable,  $T_p$  is a period of perturb,  $dx$  is the amplitude of perturbation and  $P_{pv}$  is the output power of the PV module.

## IV. SOFT COMPUTING MPPT TECHNIQUES

### A. The Fuzzy logic control (FLC) technique.

FLC MPPT is a common implementation of fuzzy logic control in modern microcontrollers for monitoring MPP. The output of the MPPT controller is evaluated and managed using fuzzy logic principles in this approach. FLC is advantageous because it can handle non-linear systems, works with approximate inputs, and doesn't necessitate a precise mathematical model. See Figure 9 for an overview of the three main building blocks that make up the FLC system: fuzzification, inference engine, and defuzzification.

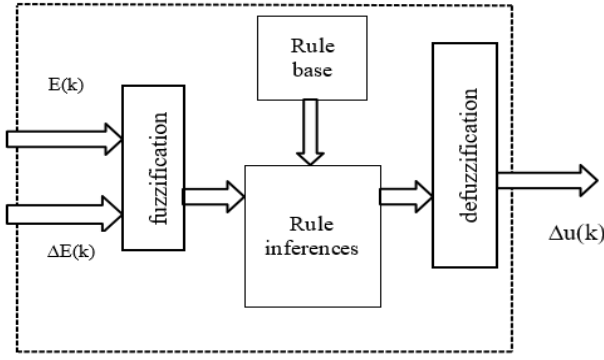


Fig. 9. The basic structure of fuzzy logic control.

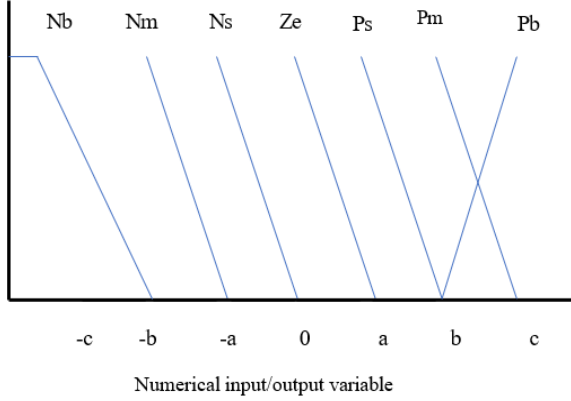


Fig. 10. membership function of input and output of FLC.

### 1) Fuzzification

Using a membership function that defines the extent of membership in one of several fuzzy subsets, the input values are first transformed into a linguistic variable in the first step of the FLC process, known as "fuzzification." The designer's skill determines the number of fuzzy subsets used, but typically seven triangular subsets are employed: positive big (PB), negative medium (NM), negative small (NS), zero (ZE), positive small (PS), and positive medium (PM) (PB). As can be seen in Figure 10, these membership functions have a visual representation.

### 1) Inference engine

The rules are applied to the fuzzy sets generated in the preceding fuzzification stage, which is followed by the inference engine, the second part of the FLC process. Here, the system determines the significance of each linguistic variable in the rule inferences and saves that information in the rule table. An FLC rule base with seven triangular membership functions is shown in Table 1.

### 2) Defuzzification

Defuzzification, the last step in FLC, transforms the linguistic variables into the membership functions' actual output values. In most cases, an FLC will have two inputs and a single output, and it will be used in an MPPT setup. The error (E) and the variation in error (E) at sampled times k, defined by equations 7 and 8, are used as input variables in FLC for MPPT.

$$E(k) = \frac{p(k) - p(k-1)}{V(k) - V(k-1)} \quad (7)$$

$$\Delta E(k) = E(k) - E(k-1) \quad (8)$$

The fuzzy logic control (FLC) method utilizes Equations 7 and 8 to define the input variables, which are power (P) and voltage (V) of PV module. The FLC system's output is the duty cycle (u) of DC/DC converter, which can be modified to fine-tune operating point of PV system. The membership functions from Table 1 are used to define the input variables. If error (E) is classified as a positive big (PB) and the change in error (DE) is classified as zero (ZE) according to rule base presented in Table (1), the FLC system's output will be PB. If operating point is distant from the MPP, the controller will increase the duty cycle to bring it closer to the MPP.

### B. Artificial neural network technique.

These algorithms are an effective method for monitoring the maximum power point of PV systems. These algorithms are built using principles of biological neural networks, which emulate the way the human brain processes information. The ANN is highly adept at complex calculations and can be trained to solve problems, making it an ideal choice for dealing with non-linear systems. Figure 11 shows the usual architecture of an artificial neural network (ANN) comprises of three layers: an input layer, a hidden layer, and an output layer. The irradiance, temperature, and open- and short-circuit currents of the solar module are some of the input parameters used by ANN in MPPT applications. The ANN's inputs can consist of any combination of these variables. The converter's output parameter is a reference signal used to determine the MPP and is typically the device's voltage, current, or duty cycle. The weight values of the connections between neurons in an ANN are chosen arbitrarily during its initial training process. When the ANN has been trained extensively, these weight values are fixed, allowing it to reliably monitor the PV system's MPP. The time required to train an ANN can range from a few days to several months or even years. During this time, the neural network's inputs and outputs are monitored for trends in order to improve its efficiency. An important drawback of using ANN for MPPT is that different PV modules can have different characteristics, so the ANN must be individually trained for each module. Furthermore, a PV module's characteristics can shift over time due to weather, necessitating frequent retraining of the neural network to guarantee precise MPPT. Tracking accuracy is algorithmically determined in the hidden layer. Increasing the number of nodes in the hidden layer can improve tracking accuracy, but it can also increase computational time and slow down tracking in some situations. Reducing the total number of nodes, on the other hand, can speed up computations but may compromise accuracy [20].

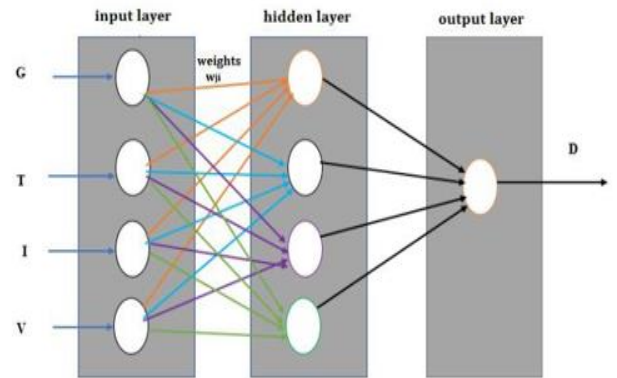


Fig. 11. ANN structure with three layers.

TABLE I. RULES-BASED THE FUZZY LOGIC CONTROLLER OF MPPT

Error (E)	Change Error (CE)						
	PB	PM	PS	ZE	NS	NM	NB
PB	PB	PB	PB	PB	PM	PS	ZE
PM	PB	PB	PB	PM	PS	ZE	NS
PS	PB	PB	PM	PS	ZE	NS	NM
ZE	PB	PM	PS	ZE	NS	NM	NB
NS	PM	PS	ZE	NS	NM	NB	NB
NM	PS	ZE	NS	NM	NB	NB	NB
NB	ZE	NS	NM	NB	NB	NB	NB

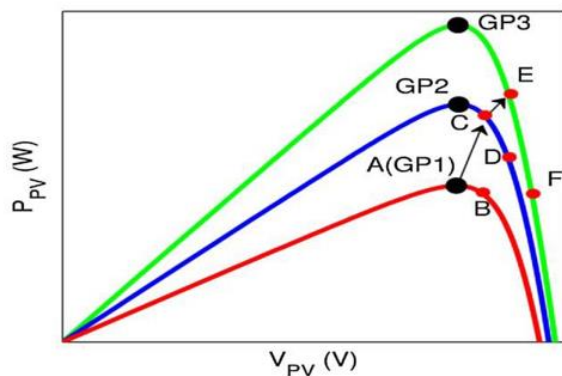


Fig. 12. P-V curve of PV module under changing irradiance [21].

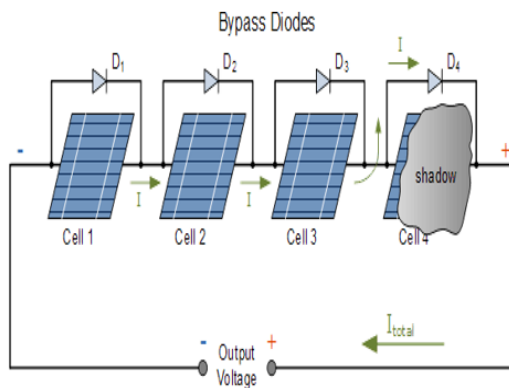


Fig. 13. one cell under partial shading.

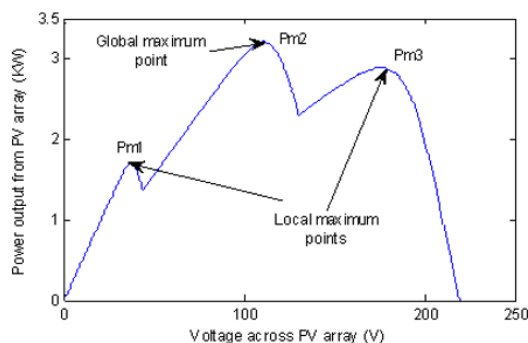


Fig. 14. The P-V curve of PV module under partial shading.

## V. CHALLENGES FACING MPPT TECHNIQUES

Both partial shading and rapid environmental change present significant difficulties for maximum power point tracking methods. When only a section of a solar panel is covered by shadow, we talk about partial shading. Because of this, it can be challenging for MPPT methods to precisely follow the MPP. When the amount of solar irradiance or temperature suddenly changes, the MPP can change just as rapidly. To keep power output at a maximum throughout these shifts, MPPT methods need to be flexible.

## VI. FAST-CHANGING IRRADIANCE CONDITION SOLUTIONS.

Since there is only one maximum power point (MPP) that can be easily detected, MPPT control algorithms perform well when the irradiance is uniform and changes slowly. However, when there are sudden shifts in irradiance, traditional MPPT methods have trouble keeping up with the MPP. This is because the PV curve can have multiple MPPs and finding them all can be difficult. Under rapidly changing irradiance, the MPPT control system might not be able to react quickly enough, reducing the photovoltaic system's efficiency. Under rapidly varying irradiance conditions, as shown in Figure 12 PV curves can have multiple maximum points. Assuming point A as the starting point, the MPPT algorithm begins tracking the MPP. If primary perturbation direction is positive and reference voltage is raised to point B, the output power is observed to increase due to an increase in irradiance, causing the operating point to move to point C. Despite moving away from the MPP, the algorithm maintains to increase the voltage. During another change in irradiance, the operating point moves from C to E, and the algorithm observes an increase in output power during this perturbation period. Consequently, the algorithm raises the reference voltage in the same direction, resulting in point F, and the operating point moves even further away from the MPP. However, this process is not very clear as the algorithm depends on the output power value and cannot differentiate whether the increase is due to the operating point traveling towards the MPP or an increase in irradiance.

### A. Partial shading condition solutions.

A drop in voltage occurs in a solar cell or group of cells whenever they are shaded by an obstruction such as a tree, a building, a cloud, or anything else (s). Failure can occur because the shaded cell(s) are now acting as a load instead of a generator. A bypass diode is used to prevent this from happening by rerouting the current away from the shaded cell(s) and into the load[22]. Figure 13 illustrates a single cell that experiences partial shading, while Figure 14 displays the P-V curve of a PV module with multiple maximum power points (MPPs) when partial shading occurs and the bypass diode is activated, resulting in global and local peaks. This is due to the shaded cells' inability to contribute to power generation, causing the operating point to shift away from the global MPP. When the operating point is at a maximum power point (MPP) of the unshaded cells, the output power is at its highest. Detecting the global peak under shading conditions can be challenging as local peaks are usually smaller than the global peak. This presents a difficulty in efficiently detecting the global peak. Most MPPT algorithms are not capable of distinguishing between local and global maximum power points, making it difficult to track the true MPP under partial shading conditions. While removing the bypass diode from the system could simplify the tracking process by reducing the number of peaks, it would also increase the cost of solar power

generation. Therefore, removing the bypass diode is not a viable solution.

### CONCLUSION

To maximize the efficiency of photovoltaic (PV) system, several maximum power point tracking (MPPT) methods were used. This paper reviews the most commonly used MPPT techniques, both soft computing and conventional methods, selected from various literary works. The paper illustrates the principle of work and implementation for each technique. The paper also discussed the challenges that face the MPPT techniques, like partial shading and fast-changing irradiance conditions. However, the choice of MPPT technique will depend on the specific application and the environmental conditions that the PV system will be exposed to. Overall, the results of this study show that MPPT techniques are a valuable tool for improving the performance of PV systems. The use of MPPT techniques can lead to significant increases in efficiency and reliability, making them a cost-effective way to increase the value of PV systems.

### CONTRIBUTION OF THE AUTHORS

The contributions of the authors to the article are equal.

### CONFLICT OF INTEREST

There is no conflict of interest between the authors.

### STATEMENT OF RESEARCH AND PUBLICATION ETHICS

Research and publication ethics were observed in this study.

### REFERENCES

- [1] M. E. Başoğlu, "Comprehensive review on distributed maximum power point tracking: Submodule level and module level MPPT strategies," *Sol. Energy*, vol. 241, pp. 85–108, 2022, doi: <https://doi.org/10.1016/j.solener.2022.05.039>.
- [2] P. Bharadwaj and V. John, "Optimized Global Maximum Power Point Tracking of Photovoltaic Systems Based on Rectangular Power Comparison," *IEEE Access*, vol. 9, pp. 53602–53616, 2021, doi: [10.1109/ACCESS.2021.3071136](https://doi.org/10.1109/ACCESS.2021.3071136).
- [3] W. Zhang, G. Zhou, H. Ni, and Y. Sun, "A Modified Hybrid Maximum Power Point Tracking Method for Photovoltaic Arrays Under Partially Shading Condition," *IEEE Access*, vol. 7, pp. 160091–160100, 2019, doi: [10.1109/ACCESS.2019.2950375](https://doi.org/10.1109/ACCESS.2019.2950375).
- [4] S. K. Cherukuri *et al.*, "Power Enhancement in Partial Shaded Photovoltaic System Using Spiral Pattern Array Configuration Scheme," *IEEE Access*, vol. 9, pp. 123103–123116, 2021, doi: [10.1109/ACCESS.2021.3109248](https://doi.org/10.1109/ACCESS.2021.3109248).
- [5] H. Delavari and M. Zolfi, "Maximum power point tracking in photovoltaic systems using indirect adaptive fuzzy robust controller," *Soft Comput.*, vol. 25, no. 16, pp. 10969–10985, 2021, doi: [10.1007/s00500-021-05823-0](https://doi.org/10.1007/s00500-021-05823-0).
- [6] A. Gani and M. Sekkeli, "Experimental evaluation of type-2 fuzzy logic controller adapted to real environmental conditions for maximum power point tracking of solar energy systems," *Int. J. Circuit Theory Appl.*, vol. 50, no. 11, pp. 4131–4145, 2022, doi: <https://doi.org/10.1002/cta.3374>.
- [7] K. Nora, A. Idir, S. Grouni, and M. S. Boucherit, "A NEW COMBINED METHOD FOR TRACKING THE GLOBAL MAXIMUM POWER POINT OF PHOTOVOLTAIC SYSTEMS," *Rev. Roum. des Sci. Tech. Série Électrotechnique Énergétique*, vol. 64, p. 2022, 2022.
- [8] Z. Kesilmiş, "A manhattan metric based perturb and observe maximum power point tracking algorithm for photovoltaic systems," *Energy Sources, Part A Recover. Util. Environ. Eff.*, vol. 44, pp. 469–492, 2022, doi: [10.1080/15567036.2022.2046662](https://doi.org/10.1080/15567036.2022.2046662).
- [9] T. Sutikno, A. C. Subrata, and A. Elkhateb, "Evaluation of Fuzzy Membership Function Effects for Maximum Power Point Tracking Technique of Photovoltaic System," *IEEE Access*, vol. 9, pp. 109157–109165, 2021, doi: [10.1109/ACCESS.2021.3102050](https://doi.org/10.1109/ACCESS.2021.3102050).
- [10] L. Tightiz, S. Mansouri, F. Zishan, J. Yoo, and N. Shafaghathian, "Maximum Power Point Tracking for Photovoltaic Systems Operating under Partially Shaded Conditions Using SALP Swarm Algorithm," *Energies*, vol. 15, p. 8210, 2022, doi: [10.3390/en15218210](https://doi.org/10.3390/en15218210).
- [11] F. Sedaghati, A. Nahavandi, M. A. Badamchizadeh, S. Ghaemi, and M. Abedinpour Fallah, "PV Maximum Power-Point Tracking by Using Artificial Neural Network," *Math. Probl. Eng.*, vol. 2012, p. 506709, 2012, doi: [10.1155/2012/506709](https://doi.org/10.1155/2012/506709).
- [12] I. Mandourarakis, V. Gogolou, E. Koutroulis, and S. Siskos, "Integrated Maximum Power Point Tracking System for Photovoltaic Energy Harvesting Applications," *IEEE Trans. Power Electron.*, vol. 37, no. 8, pp. 9865–9875, 2022, doi: [10.1109/TPEL.2022.3156400](https://doi.org/10.1109/TPEL.2022.3156400).
- [13] S. Mumtaz, S. Ahmad, L. Khan, S. Ali, T. Kamal Khan, and S. Hassan, "Adaptive Feedback Linearization Based NeuroFuzzy Maximum Power Point Tracking for a Photovoltaic System," *Energies*, vol. 11, p. 606, 2018, doi: [10.3390/en11030606](https://doi.org/10.3390/en11030606).
- [14] R. K. Phanden, L. Sharma, J. Chhabra, and H. İ. Demir, "A novel modified ant colony optimization based maximum power point tracking controller for photovoltaic systems," *Mater. Today Proc.*, vol. 38, pp. 89–93, 2021, doi: <https://doi.org/10.1016/j.matpr.2020.06.020>.
- [15] M. Shamseldin, "Unconstrained model and merge sorted serpentine arrangement method for dynamic reconfiguration of large PV arrays," *Energy Convers. Manag.*, vol. 16, p. 100320, 2022, doi: <https://doi.org/10.1016/j.ecmx.2022.100320>.
- [16] R. Roupahel, N. Maamri, and J.-P. Gaubert, "Dynamic Maximum Power Point Tracking Method including Detection of Varying Partial Shading Conditions for Photovoltaic Systems," in *2022 24th European Conference on Power Electronics and Applications (EPE'22 ECCE Europe)*, 2022, pp. 1–8.
- [17] U. C. Turhal and Y. Onal, "Maximum Power Point Estimation Based on Operating Conditions Classification for Photovoltaic Systems: A Case Study for Partial Shading," *Acta Phys. Pol. A*, vol. 142, no. 2, pp. 256–265, 2022, doi: [10.12693/APhysPolA.142.256](https://doi.org/10.12693/APhysPolA.142.256).
- [18] M. H. Osman, M. K. Ahmed, A. Refaat and N. V. Korovkin, "A Comparative Study of MPPT for PV System Based on Modified Perturbation & Observation Method," *2021 IEEE Conference of Russian Young Researchers in Electrical and Electronic Engineering (ElConRus)*, St. Petersburg, Moscow, Russia, 2021, pp. 1023–1026, doi: [10.1109/ElConRus51938.2021.9396444](https://doi.org/10.1109/ElConRus51938.2021.9396444).
- [19] A. B. M. I. F.-B. A. Y. A. Roberto I. Rico-Camacho Luis J. Ricalde, "Transient Differentiation Maximum Power Point Tracker (Td-MPPT) for Optimized Tracking under Very Fast-Changing Irradiance: A Theoretical Approach for Mobile PV Applications," *Appl. Sci.*, vol. 12, no. 5, p. 2671, 2022, doi: [10.3390/app12052671](https://doi.org/10.3390/app12052671).
- [20] U. ur Rehman, P. Faria, L. Gomes, and Z. Vale, "Artificial Neural Network Based Efficient Maximum Power Point Tracking for Photovoltaic Systems," in *2022 IEEE International Conference on Environment and Electrical Engineering and 2022 IEEE Industrial and Commercial Power Systems Europe (EEEIC / I&CPS Europe)*, 2022, pp. 1–6, doi: [10.1109/EEEIC/ICPSEurope54979.2022.9854613](https://doi.org/10.1109/EEEIC/ICPSEurope54979.2022.9854613).
- [21] A. F. Mirza, M. Mansoor, K. Zhan, and Q. Ling, "High-efficiency swarm intelligent maximum power point tracking control techniques for varying temperature and irradiance," *Energy*, vol. 228, p. 120602, 2021, doi: <https://doi.org/10.1016/j.energy.2021.120602>.
- [22] K. Unal, G. Bal, S. Oncu, and N. Ozturk, "MPPT Design for PV-Powered WPT System with Irregular Pulse Density Modulation," *Electr. Power Components Syst.*, vol. 51, no. 1, pp. 83–91, 2023, doi: [10.1080/15325008.2022.2161674](https://doi.org/10.1080/15325008.2022.2161674).

# The Viability and Cost-Effectiveness of Hybrid Renewable Energy Systems in Rural Areas

Received: 10 May 2023; Accepted: 28 June 2023

Research Article

Abdullah Abodwair  
Karabuk university  
Department of electrical and electronic engineering  
Karabuk, Turkey  
2138171025@orgenci.karabuk.edu.tr  
0000-0000-0000-0000

**Abstract**— This research aims to develop a computer model of a hybrid renewable energy system that can operate independently for a faculty of engineering of Karabuk university, located in Turkey. The hybrid system consists of several components, such as Photovoltaic (PV) panels, wind turbines, diesel generator, and battery storage system as a backup. The primary purpose of this system is to meet the energy needs of a university building. Different combinations of the hybrid system were examined using HOMER software to determine the most cost-efficient solution based on the net present cost. Following the analysis of multiple combinations, the optimal hybrid system was determined, which consists of a 500kW PV system, wind turbines with a total capacity of 7.5MW, and a 327Ah, 15.7kw/h battery storage system, diesel generator of 2000 kw. The overall cost of the system \$693,000,000, the project lifespan is 25 years.

**Keywords**— Hybrid energy system, HOMER, PV-Wind-Battery, diesel generator.

## I. INTRODUCTION

Hybrid power systems that combine conventional and renewable energy sources are becoming increasingly popular, particularly in remote areas where traditional energy sources may not be available. These systems utilize renewable sources like solar and wind power to reduce dependence on fossil fuels and promote sustainable development while ensuring a reliable electricity supply[1]. Battery storage systems play an important role in these hybrid systems, helping to provide electricity to consumers when renewable sources are unable to meet the load demand due to intermittent resources. In a hybrid system, PV, wind turbines, and diesel generator systems work together to meet the load demand. To address the energy issues, researchers are exploring the potential of hybrid energy systems to provide reliable electricity supply. In a study focused on Karabuk university, faculty of engineering building located in Karabuk, Turkey, researchers assessed the feasibility of using PV and wind turbines as the main power sources, with a backup system from diesel generator, and battery storage. They used HOMER software to determine the optimal hybrid system configuration based on several crucial parameters, such as the availability of renewable resources and the project cost.[2].

HOMER analyzed the specific arrangement of the system components in terms of component sizing and operating scheme over a particular project lifecycle, and then ranked the system configuration output based on its total net present cost. The results of the study could serve as a benchmark for other sites looking to implement alternative energy sources[3]. The system is comprised of a PV array, wind turbine, power converter, diesel generator, and batteries with different capacities.

## II. LITERATURE REVIEW

In order to build hybrid renewable energy systems (HRES) that take into account the possible resources that may be available at a particular place, software called HOMER is commonly used. Numerous research have been done in relation to the techno-economic analysis and design of HRES [4]. The design of the Hybrid Renewable Energy System (HRES) will be based on a comprehensive evaluation of both technical and economic performance criteria to determine the optimal solution. [5]. In terms of technical performance, The best possible renewable fraction should be applied to the ideal HRES design, which is the ratio of renewable energy sources to the total energy generated, and the lowest proportion of yearly unmet load. The annual unmet load percentage represents the amount of energy demand that is not met by the HRES. These technical performance criteria ensure that the HRES can meet the energy demand of remote areas without access to grid sources[6]. On the economic front, the HRES with the least leveled cost of electricity (COE), which is the total cost of electricity generation over the lifetime of the HRES, and minimum net present cost (NPC) is preferred. The economic performance criteria ensure that the HRES is affordable and sustainable for remote areas. If the HRES design satisfies both the technical and economic performance criteria, then this optimized hybrid system is well-suited for providing electricity to rural areas that are located beyond the reach of traditional grid sources, making it an ideal solution for remote electrification efforts. It is recommended for implementation in such areas. [7].

The use of HOMER software and related research can help inform policymakers and energy planners in making informed decisions for rural electrification projects. Additionally, numerous research studies have been undertaken To study the technological economic design of hybrid clean energy systems[8]. For example, in one study cited as Reference [9], a hybrid system which consists of battery storage, solar energy, and biogas, and a power converter was The implemented system aimed to provide electricity and cooking solutions in rural region of Bangladesh. The study revealed that an optimal hybrid system could be achieved with 0.2 kW-PV, The hybrid system consisted of a 250 W solar panell, a 0.3 kW electrical power converters and a 0.6 kW biogas engine ,three 360 Ah batteries, demonstrating its ability to provide electricity to households in isolated regions, and making sure that 73% of the system's generated biogas had been used for cooking.. Such research studies provide valuable insights into the design and optimization of hybrid renewable energy systems for rural electrification projects[10]. By using the knowledge gained from these studies, policymakers and energy planners can make informed decisions on the deployment of HRES to ensure sustainable

and affordable electricity access in remote areas. An HRES with a COE of 0.384 \$/kWh has been found to be the most cost-effective option for fulfilling the energy needs of rural communities in Bangladesh, based on a study detailed in Reference[11]. In Reference [12], A research team conducted an investigation into the viability and deployment of hybrid grid-interactive energy produced from renewable sources system techno-economic aspects (HGIRES) in a rural area of Egypt[12]. The study evaluated multiple system configurations, HOMER Pro software was utilized to assess various parameters, for a load demand of 48 kW, taking into account COE, NPC, the proportion of renewable energy, the percentage of unmet load, and emission levels. The findings demonstrated that the PV/DG/converter arrangement offered the best technical performance, cost-effectiveness, and environmental sustainability for the given location. This system boasted the lowest COE of 0.139 \$/kWh, a significant improvement over a DG-only system. Reference [2] the study analyzed a range of system configurations for a hybrid renewable energy system that included PV panels, wind turbines, fuel cells, a diesel generator, converters, and batteries for storage. Seasonal variations in load demand were taken into account, and the research was carried out with the aid of HOMER software. According to the research. The most practical and efficient alternative to other system concepts was the combination of the solar/Wind/Fuel cell/Diesel-generator/Converter system [13]. A novel hybrid power system has been proposed for meeting the daily energy demands of households in the coastal regions of Turkey[14]. This innovative system effectively balances the need for reliable power supply with cost-effectiveness and environmental sustainability, achieving a remarkable 95% renewable energy fraction while minimizing the levelized (COE) to \$0.282/kWh and the (NPC) to \$253,590. Furthermore, to address future energy challenges, the study suggests the implementation of a 15 MW Saudi Arabia wind energy system [9]. This strategic move would not only reduce the COE but also enable the country to tap into its immense wind energy potential, thereby ensuring a sustainable energy future for the region. By adopting such innovative and sustainable approaches, we can pave the way for a greener and more equitable world. According to the estimates, the cost of generating power through wind turbines for the Khamis-Mushayt region is \$0.1016 per kWh, whereas it is \$0.0612 per kWh for the Badanah region [15]. The research is based on the ability of wind energy to meet the total annual load demand of 33.37 kWh/d in these regions. Wind energy has the potential to be a cost-effective and sustainable solution for meeting the energy needs of these areas. By harnessing the power of wind, we can create a cleaner and more sustainable future while simultaneously meeting the growing energy demands of our communities[11].

In Reference [8]. In their research published , In order to develop and plan hybrid energy systems that combine a systematic framework combining wind, solar power, biomass, fossil fuels, and battery systems., with the aim of achieving low carbon emissions. These systems have been specifically designed for urban electrification in Canada. The study highlights that the cost of energy (COE) for the The cost of a PV/wind/biomass system is three times lower than that of a solar/wind hybrid system. Given the variability and uncertainty in input variables, the authors have employed three sensitivity parameters, which include the discount rate, PV panel capital cost, and storage capital cost, to accurately

calculate the COE for these models. The study offers valuable insights for policymakers to create effective urban hybrid system policies and procedures. Additionally, the research also indicates that incorporating low-carbon natural gas generators into the design of the PV/wind/biomass system can reduce the cost of electricity by nearly 30%, making it a viable alternative to traditional natural gas power plants. These findings are crucial in enabling policymakers to make informed decisions about designing and implementing hybrid energy systems that are both cost-effective and environmentally sustainable. In Reference[16], the authors have proposed a model predictive control method aimed to improve energy demand management by balancing power between both generation and consumption and lowering the system's total operating costs. To achieve this, they utilized an autoregressive average model to estimate the values of wind power production, load demand, and tariffs for electricity.

The researchers also examined the unpredictability of electricity prices using a method called conditional value at risk. From the reviewed literature, it was noted that utilizing hybrid renewable energy systems, the difficulties of providing uninterrupted electricity to rural areas are unable to be resolved by a single power source, but a combination of sources, such as those utilizing biomass, solar, and wind energy technology, can be more dependable. One of the most effective hybrid systems for remote rural areas with abundant solar irradiation is the PV/diesel generator/battery/converter model, while the wind energy/diesel generator/battery/converter model is ideal for areas with high wind potential availability.

The HOMER software was used to design optimal hybrid systems, with a COE ranging from \$0.054 to \$0.588 per kWh. The most suitable system Future electrification should aim for the lowest COE, lowest NPC, the most significant proportion of renewable energy, lowest carbon emission, and absolutely no unmet load. Many ongoing research studies are focused on developing optimal hybrid renewable energy systems, including both renewable and conventional energy sources, for both grid-connected and standalone systems.

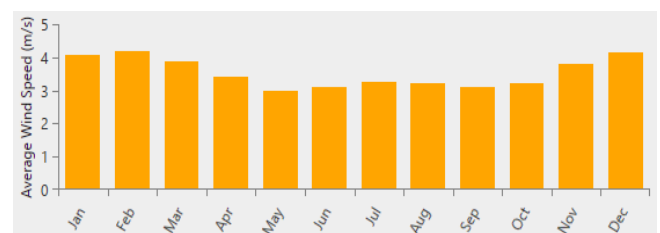


Fig. 1. Monthly wind speed



Fig. 2. Monthly solar radiation

### III. RESEARCH METHOD

#### A. Simulation

The research conducted a simulation using HOMER software to optimize a hybrid system consisting of a photovoltaic (PV) array, wind turbine, diesel generator, and Battery bank for Karabuk university, faculty of engineering in Turkey. During the simulation process, input data, such as solar radiation, wind speed, and load demand, were used to establish the system configuration, which was ranked by net present cost (NPC). The building is located in Karabuk city in Turkey at 41°12'70 latitude and 32° 39'14 longitude. Using HOMER software, the researchers simulated a hybrid system composed of PV, wind, diesel generator, and battery storage. To optimize the system configuration based on net present cost (NPC), the software considered various inputs, including solar radiation, wind speed, and load demand, which were estimated from the system's location [13].

#### B. Wind speed

According to data gathered from NASA Surface Meteorology and Solar Energy between 1984 to 2013, the average monthly wind speed at a height of 50 meters is 3.54 m/s. December has the highest wind speed with a maximum of 4.13 m/s, while May has the lowest with a minimum of 3.0 m/s. Figure 1 provides a graphical representation of these wind speed variations throughout the year. [17][9].

#### C. Solar radiation

Based on the information displayed in Figure 2, the village has an average daily solar radiation of 3.99 kWh/m<sup>2</sup> from 1983 to 2005. The highest solar radiation levels are observed in July, reaching 6.9 kWh/m<sup>2</sup>/day, while the lowest levels are recorded in December with only 1.28 kWh/m<sup>2</sup>/day[18].

#### D. Load demand

The estimation of the load demand for the faculty of engineering building was carried out by analyzing the customary energy consumption patterns of individual offices and laboratory inside the building, revealing that the highest demand of 1576.62 kW transpires in January, and the average load is 1089.5 kW. Figure 3 illustrates the monthly load profile for the building, which exhibits the highest demand during the year. HOMER, the software utilized for this analysis, generates a load profile with a normal distribution of a mean of 1 and a standard deviation of 20% to simulate the actual load profile[11].

at this location to cater to the escalating to ensure a reliable electricity supply that meets the required load demand [20].

#### B. Wind system

To simulate the hybrid power system, the Enercon [7.5MW] wind turbine was chosen with a rated power of 7580 kW, an asynchronous generator. The wind turbine illustrated in Figure 6 has a rotor diameter of 127 meters, and it is installed at a hub height of 135 meters. Table 1 outlines the economic and technical specifications of the turbine. [6]. The estimated capital cost for a single wind turbine is \$187,000/kW [12], and it is projected to decrease by 17% from 2022 to 2030, resulting in a replacement cost of \$156,000 [12]. The annual cost of operation and maintenance for a wind turbine is \$12,500/kW [13].

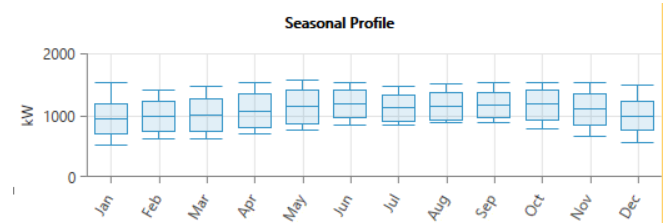


Fig. 3. Load profile

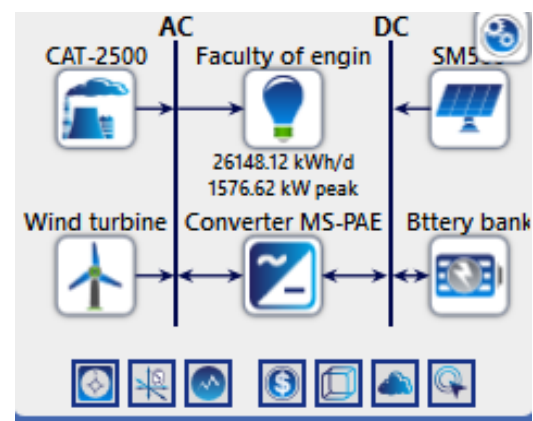


Fig. 4. Hybrid system configuration using HOMER

### IV. HYBRID SYSTEM DESIGN

The recommended system design involves the combination of a photovoltaic (PV) array and a wind turbine system as the main sources of renewable energy for generating electricity. A diesel generator, and battery storage system is also integrated to serve as a backup power source, ensuring a reliable supply of electricity[19]. Figure 4 displays the configuration of the hybrid system as modeled in HOMER software[20].

#### A. Bulding site detail

This study focuses on a site situated in Turkey ,faculty of engineering, Karabuk university, the building is located at 41° 12'49 latitude and 32° 39'14 longitude, as depicted in Figure 5. Although grid power is available, it is inadequate to meet the rising demand, especially during the winter months. Therefore, it is necessary to construct a hybrid power system



Fig. 5. Geographic map of the study area

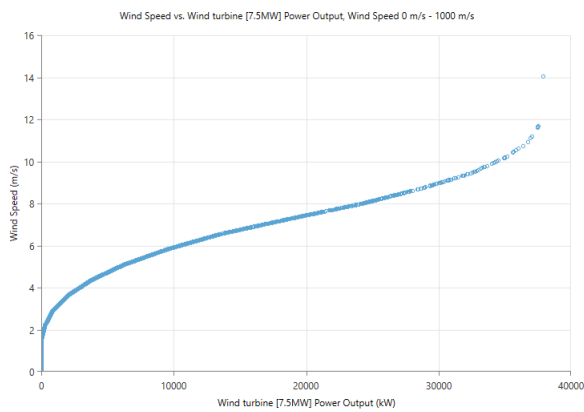


Fig. 6. Wind turbine power curve





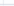
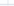



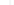





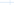
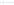
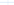
Optimization Results												Compare Economic	Columns Choiced		
Left Double Click on a particular system to see detailed Simulation Results.												Categorized			
Architecture												Cost		System	
  	SM500 (kW)	SM500-MPPPT (kW)	Wind turbine (kW)	CAT-2500 (kW)	Battery bank (Ah)	Converter MS-PAE (kW)	Dispatch (kW)	NPC (\$)	LCOE (\$/kWh)	Operating cost (\$/yr)	CAPEX (\$)	Net Fnc (\$)	Total Fuel (\$/yr)		
  	5		5	2,000	43	440	CC	\$693M	\$5.62	\$53.3M	\$3.97M	60.4	1,144,935		
  	5		5	2,000	43	440	CC	\$693M	\$5.62	\$53.3M	\$3.97M	60.4	1,144,935		
  	500	500	5	2,000	26	440	CC	\$107M	\$5.73	\$53.3M	\$17.8M	60.5	1,143,708		
  	500	500	5	2,000	26	440	CC	\$107M	\$5.73	\$53.3M	\$17.8M	60.4	1,144,376		
  				2,000			CC	\$1,178	\$9.46	\$90.3M	\$240,000	0	2,671,648		

Fig. 7. Categorized optimization results for diesel price of 0.1 \$/L

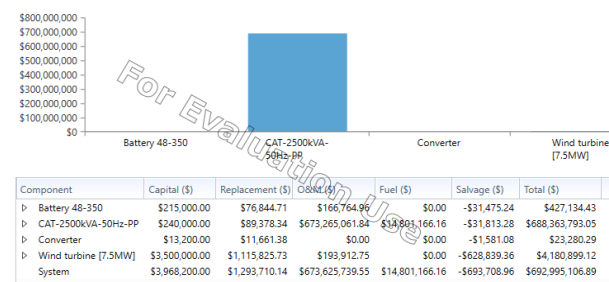


Fig. 8. Hybrid system NPC

TABLE I. TECHNICAL AND ECONOMIC DETAILS OF THE WIND TURBINE

Description	Specification
Producer	Enercon
Rotor diameter	127 M
Hub height	135 M
Lifecycle	20 years
Nominal voltage	230/400 V (AC)
Cut out wind speed	28-34 M/sec
Capital Cost	\$700000
Replacement Cost	\$700000
O&M Cost	3000 \$/year
Rated power	7580 kW

### A. Diesel generator

The selected diesel generator CAT-2000kw-50Hz, with capital cost of \$240,000, operation cost \$/yr 673,000, considering that the fuel price is 1 \$/L.

### B. Pv system

As per the Q1 2022 report by the National Renewable Energy Laboratory (NREL), the capital cost for installing and replacing a PV system is \$56/kW. The operation and maintenance costs for the PV system are \$10/year [21, 22]. The PV system used in this study has a capacity of 500 kW and a lifetime of 20 years, with no tracking system. Table 2 displays the technical specifications of the PV modules.

### C. Battery

For the proposed hybrid system, the selected storage battery is the Kinetic 15.7kWh battery, which has a rated capacity of 327 Ah and a rated voltage of 48 V. The battery can store up to 1 kWh of energy. The initial cost for one unit of this battery is \$5000, with a replacement cost of \$5000 as well. The annual cost for operation and maintenance is estimated to be \$300, according to [5] [20].

### D. Power converter

The selected converter for the proposed hybrid system is the converter SM-PAE 120/240V, which has a step range size of 1,000 kW and a maximum capacity of 17.6 kW. The converter has an efficiency of 94%, an initial cost of \$3000/kW, and a lifespan of 10 years.

## V. RESULTS AND DISCUSSION

The HOMER software runs simulations for all the systems to determine the most cost-effective option that can meet the electricity load demand.

### A. Optimization results

The HOMER software generated the top ten optimized outcomes for cost efficiency, as depicted in Figure 7. The selected hybrid system that satisfies the economic feasibility criteria consists of five units of 7580 kW wind turbine, a 17.6 kW power converter, diesel generator with 2000kW capacity, and a 43 battery with a 327 Ah capacity [14].

### B. Cash flow summary results

According to the results generated by HOMER software, a hybrid system that integrates 5 units of wind turbines, a power converter, and a 43 batteries storage system would have a total Net Present Cost (NPC) of \$693,000,000. The operating and maintenance cost would be approximately \$674,000,000. As a result, the cost of energy produced by this system is estimated to be 5.62 \$/kWh. The wind turbine system is the most expensive component of the hybrid system, costing \$3,500,000, which is attributed to the high price and capacity of the wind turbines. The second most expensive component is the diesel generator, with a cost of \$240,000. Figure 8, and table 3 explains the NPC of the proposed hybrid system.

TABLE II. SPECIFICATION OF SOLAR PV ARRAY

Description	Specification
Manufacturer	Generic
Solar Cells	Flat plate
Module Number	SM500
Nominal Power	500kW
Average Panel Efficiency	17.3%
Max. System Voltage	600 V
Capital Cost	56 \$/kW
Replacement Cost	10 \$/kW

TABLE III. SPECIFICATION OF SOLAR PV ARRAY

Net Present Value	\$474M
Capital Investment	\$3.73M
Annualized Savings	\$37.0M

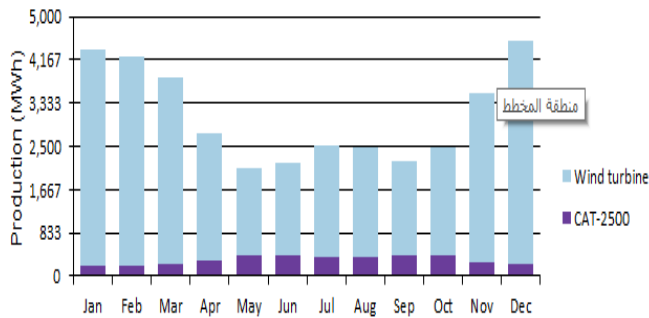


Fig. 9. Monthly average electric production

### C. Finding of Energy production

Figure 9 illustrates the monthly average electric production of a hybrid system that generates a total of 37,130,595 kWh/year. The results indicate that the PV system contributes zero kWh/yr, while the wind turbines generate 33,351,963 kWh/yr, representing 89.8% of power generation. While the diesel generation produced electricity of 3,778,632 kWh/yr, which representing of 10.2% of total energy production.

The excess electricity generated by the hybrid system is 27,586,531 kWh/yr, indicating that the system produces more electricity than the total demand. Additionally, the unmet load capacity is estimated to be 0.0 kWh/yr. [23]. The total renewable production representing of 89.8% of the proposed hybrid system electricity production.

### CONCLUSION

The present study employed the HOMER software for simulating a hybrid system that integrates photovoltaic (PV) panels, wind turbines, diesel generator, and battery storage. By optimizing the analysis, the study identified the top ten optimal combinations of system components based on their net present cost (NPC). The most cost-effective system configuration was found to consist of a 33.351.963kW Enercon E-126 wind turbine, Generic 1MWh of 43 batteries, and MS-PAE 17.6 kW power converter, diesel generation produced electricity of 2000kw.

The study has shown that there is no benefit in using solar panels as the first two options for the hybrid system, while It is possible to use the solar system in the third proposed option according to HOMER software simulation results by installing 500 solar panels, but this will increase the initial cost of the project see Figure 7. This hybrid system was designed to provide electricity to the faculty of engineering building in Karabuk university in Turkey with the least cost possible. The study demonstrates the potential of alternative energy sources to generate electricity in Turkey.

### ACKNOWLEDGEMENT

The authors express their gratitude to Karabuk University for providing support for this research.

### CONTRIBUTION OF THE AUTHORS

The contributions of the authors to the article are equal.

### CONFLICT OF INTEREST

There is no conflict of interest between the authors.

### STATEMENT OF RESEARCH AND PUBLICATION ETHICS

Research and publication ethics were observed in this study.

### REFERENCES

- [1] A. Aksoy, "Integrated model for renewable energy planning in Turkey," *International journal of green energy*, vol. 16, no. 1, pp. 34-48, 2019.
- [2] M. Gökçek, "Integration of hybrid power (wind-photovoltaic-diesel-battery) and seawater reverse osmosis systems for small-scale desalination applications," *Desalination*, vol. 435, pp. 210-220, 2018.
- [3] Y. Gu, D. Wang, Q. Chen, and Z. Tang, "Techno-economic analysis of green methanol plant with optimal design of renewable hydrogen production: A case study in China," *International Journal of Hydrogen Energy*, vol. 47, no. 8, pp. 5085-5100, 2022.
- [4] Z. Abdin and W. Mérida, "Hybrid energy systems for off-grid power supply and hydrogen production based on renewable energy: A techno-economic analysis," *Energy Conversion and management*, vol. 196, pp. 1068-1079, 2019.
- [5] V. B. Román, G. E. Baños, C. Q. Solís, M. Flota-Bañuelos, M. Rivero, and M. E. Soberanis, "Comparative study on the cost of hybrid energy and energy storage systems in remote rural communities near Yucatan, Mexico," *Applied Energy*, vol. 308, p. 118334, 2022.
- [6] Y. T. Yürek, M. Bulut, B. Özyörük, and E. Özcan, "Evaluation of the hybrid renewable energy sources using sustainability index under uncertainty," *Sustainable Energy, Grids and Networks*, vol. 28, p. 100527, 2021.
- [7] Z. O. Al-Lababneh, "Utilizing solar cell systems in remote desert areas in Jordan to exploit sustainable energy for irrigation and agriculture," *Journal of Applied Science and Engineering*, vol. 24, no. 5, pp. 693-697, 2021.
- [8] M. Bagheri, S. H. Delbari, M. Pakzadmanesh, and C. A. Kennedy, "City-integrated renewable energy design for low-carbon and climate-resilient communities," *Applied energy*, vol. 239, pp. 1212-1225, 2019.
- [9] M. M. Rahman, M. M. Hasan, J. V. Paatero, and R. Lahdelma, "Hybrid application of biogas and solar resources to fulfill household energy needs: A potentially viable option in rural areas of developing countries," *Renewable Energy*, vol. 68, pp. 35-45, 2014.
- [10] A. C. Duman and Ö. Güler, "Techno-economic analysis of off-grid photovoltaic LED road lighting systems: A case study for northern, central and southern regions of Turkey," *Building and environment*, vol. 156, pp. 89-98, 2019.
- [11] K. Murugaperumal, S. Srinivasan, and G. S. Prasad, "Optimum design of hybrid renewable energy system through load forecasting and different operating strategies for rural electrification," *Sustainable Energy Technologies and Assessments*, vol. 37, p. 100613, 2020.
- [12] S. M. Dawoud, X. N. Lin, J. W. Sun, M. I. Okba, M. S. Khalid, and A. Waqar, "Feasibility study of isolated PV-wind hybrid system in Egypt," in *Advanced Materials Research*, 2015, vol. 1092: Trans Tech Publ, pp. 145-151.
- [13] A. C. Duman and Ö. Güler, "Techno-economic analysis of off-grid PV/wind/fuel cell hybrid system combinations with a comparison of regularly and seasonally occupied households," *Sustainable Cities and Society*, vol. 42, pp. 107-126, 2018.
- [14] C. Erdin and G. Ozkaya, "Turkey's 2023 energy strategies and investment opportunities for renewable energy sources: Site selection based on electre," *Sustainability*, vol. 11, no. 7, p. 2136, 2019.
- [15] J. O. Oladigbolu, M. A. Ramli, and Y. A. Al-Turki, "Feasibility study and comparative analysis of hybrid renewable power system for off-grid rural electrification in a typical remote village located in Nigeria," *IEEE Access*, vol. 8, pp. 171643-171663, 2020.
- [16] M. Tavakoli, F. Shokridehaki, M. Marzband, R. Godina, and E. Pouresmaeil, "A two stage hierarchical control approach for the optimal energy management in commercial building microgrids based on local wind power and PEVs," *Sustainable Cities and Society*, vol. 41, pp. 332-340, 2018.
- [17] <https://www.earthdata.nasa.gov/topics/atmosphere/atmospheric-winds/surface-winds/wind-speed>.

- <https://www.earthdata.nasa.gov/topics/atmosphere/atmospheric-winds/surface-winds/wind-speed> (accessed).
- [18] <https://solarsystem.nasa.gov/>. [Online] Available: <https://solarsystem.nasa.gov/>
- [19] S. Seker and C. Kahraman, "Socio-economic evaluation model for sustainable solar PV panels using a novel integrated MCDM methodology: A case in Turkey," *Socio-Economic Planning Sciences*, vol. 77, p. 100998, 2021.
- [20] <https://www.homerenergy.com/products/pro/index.html> (accessed May 2023.)
- [21] Ş. Emeç and G. Akkaya, "Techno-economic analysis of a university's electrical energy consumption with hybrid systems," *Journal of Information and Optimization Sciences*, vol. 42, no. 2, pp. 417-430, 2021.
- [22] C. Li, "Techno-economic study of off-grid hybrid photovoltaic/battery and photovoltaic/battery/fuel cell power systems in Kunming, China," *Energy Sources, Part A: Recovery, Utilization, and Environmental Effects*, vol. 41, no. 13, pp. 1588-1604, 2019.
- [23] S. Polat and H. Sekerci, "The determination of optimal operating condition for an off-grid hybrid renewable energy based micro-grid: A case study in Izmir, Turkey," *EMITTER International Journal of Engineering Technology*, vol. 9, no. 1, pp. 137-153, 2021.

# Using ANFIS to Predict the Long and Short Term Stroke Risk Based on Ultrasound Carotid Imaging and Clinical data of Initially Asymptomatic Patients

Received: 10 May 2023; Accepted: 28 June 2023

Research Article

Suhail Odeh  
dept. of Software Engineering  
Bethlehem University  
Bethlehem, Palestine  
sodeh@bethlehem.edu  
0000-0003-4186-8327

Efthymou Kyriacou  
dept. of Computer Science and  
Engineering  
Frederick University  
Lemesos, Cyprus  
e.kyriacou@frederick.ac.cy  
0000-0002-4589-519X

Constantinos S. Pattichis  
dept. of Computer Science  
University of Cyprus  
Nicosia, Cyprus  
pattichi@ucy.ac.cy  
0000-0000-0000-0000

**Abstract**—The aim of this study is to investigate the development of predictive modelling in order to estimate the short (less or equal to three years) or long term (more than three years) stroke risk of patients with asymptomatic carotid artery stenosis. Data were collected from 108 patients that had a stroke event have been used. The prediction is done using base line data where patients were still asymptomatic. The information collected includes non-invasive ultrasound images of the carotid arteries and several other clinical data like patient's blood tests (Cholesterol, creatinine, general blood parameters), diabetes, smoking, family history. Ultrasound images were analyzed and several features that can be used in order to characterize the type, size, structure and morphology of the atherosclerotic plaques were extracted. Based on the extracted image features and clinical data; we had created a risk modelling system based on Adaptive Network based Fuzzy Inference System (ANFIS). Model was investigated to classify the subjects into the two classes i) short ( $\leq 3$  years) and ii) long term ( $> 3$  years) period stroke events. The ANFIS could give us correct classification rate up to  $97 \pm 2.6\%$ . These results can clearly indicate that ultrasound image plaque characteristics in combination with clinical data can be used in order to create predictive models for stroke risk period.

**Keywords**— Adaptive Network based Fuzzy Inference System (ANFIS), stroke risk, Feature Selection.

## I. INTRODUCTION

Atherosclerosis of the internal carotid artery (ICA) is an important risk factor for stroke. Using the NASCET method [1] for the determination of stenosis the risk of stroke has been shown to range between 0.1-1.6% per year for asymptomatic individuals with ICA stenosis  $< 75$ -80%. The risk rises to 2-3% per year for individuals with higher grades of stenosis [2][9]. In the past three decades carotid endarterectomy was extensively used for the reduction of stroke risk. This is because two randomized controlled trials, almost a decade apart, the ACAS in 1995 [3] and the ACST in 2004 [4] reported that in patients with asymptomatic ICA stenosis  $> 60$ -70% (using the NASCET method) carotid endarterectomy reduced the risk of stroke from 2% to 1% per year [4], [5]. However, in these trials carotid endarterectomy was associated with a 2-3% perioperative rate of stroke or death making it marginally effective for asymptomatic patients. It should also be noted that in these trials, medical therapy, which was left to the discretion of the local teams, was suboptimal in relation to current practice. Recent advances in the management of vascular disease and particularly the use of statins appear to

have reduced stroke rate to approximately 1% per year and have prompted doubt regarding the value of endarterectomy in asymptomatic patients [6], [7], [9]. In addition, medical therapy was found to be 3 to 8 times more cost effective than surgical [8], [9]. However, we believe that carotid endarterectomy can still be justified if subgroups at increased risk can be identified. This raises the need for the establishment of methods for reliable and objective cerebrovascular risk prediction and stratification [9].

Non-invasive ultrasound imaging provides information not only on the degree of carotid artery stenosis but also on the characteristics of the arterial wall including the size and consistency of atherosclerotic plaques [10]. Carotid stenosis alone has limitations in predicting risk and does not show plaque vulnerability and instability, thus other ultrasonographic plaque morphologic characteristics have been studied for better prediction of risk stroke. Plaque echogenicity as assessed by B-mode ultrasound has been found to reliably predict the content of soft tissue and the amount of calcification in carotid plaques.

Additionally, it has been reported that subjects with echolucent atherosclerotic plaques have increased risk of, ischemic cerebrovascular events [10]. Most recently [11], [12], [16] showed that plaque echolucency can be used to predict stroke. Other studies have reported that plaques that are more echolucent and heterogeneous are often associated with higher cerebrovascular risk and the development of ipsilateral neurological symptoms [13], [14]. In contrast, homogeneous hypoechoic and hyperechoic plaques without evidence of ulceration usually remain asymptomatic.

Prediction of risk is important, as it will aid clinicians in the selection of asymptomatic cases at higher risk. Equally important is the establishment of a method that will allow evaluation of objective, quantitative and urgency of high-risk cases. These results will help identify the ones that would most benefit from endarterectomy. This paper aims towards the development of predictive modeling to identify group of patients that are at high risk of stroke in a short-term period ( $\leq 3$  years) as opposed to group of patients that are at a high risk of stroke in long term ( $> 3$  years). This threshold was selected based on the initial statistical analysis of the data set collected from a multicenter cohort study called Asymptomatic Carotid Stenosis and Risk of Stroke (ACSRS) [2]. Several image analyses as well as clinical features were extracted from the patients.

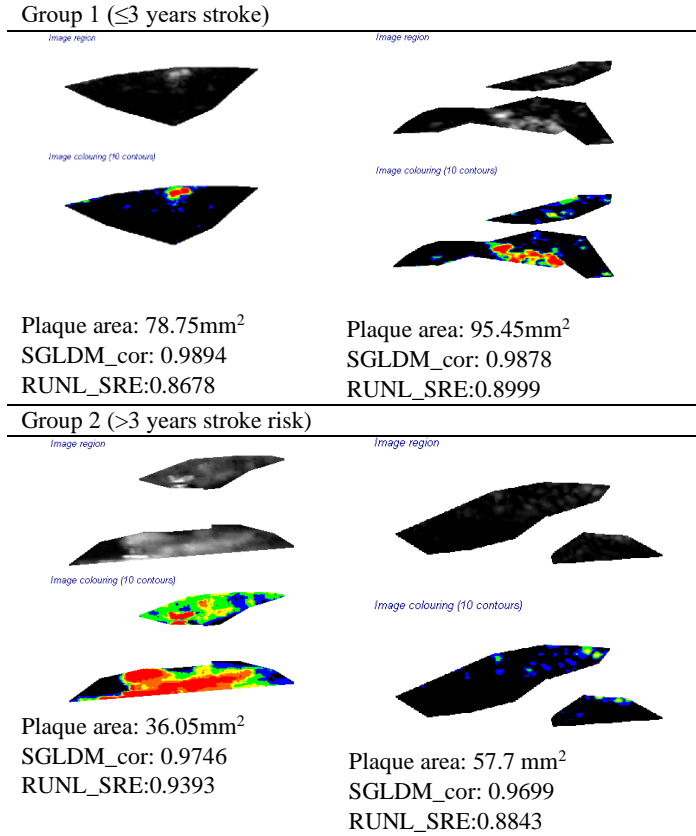


Fig. 1. Example of selected plaques at baseline, using b-mode ultrasound images and colour contoured plaques with selected

TABLE I. NUMBER OF ASYMPTOMATIC AND STROKE (INCLUDING TIA'S) CASES, SEPARATED INTO SUBGROUPS ACCORDING TO ECST STENOSIS AND NASCET STENOSIS. FOLLOW-UP 6 MONTHS TO 8 YEARS (MEAN, 48 MONTHS) [2]. GROUPS OF YEARS OF EVENT ARE FOR  $\leq 3$  YEARS GROUP ONE AND  $> 3$  YEARS GROUP TWO.

ECST st(%)	NASCET st(%)	No.	Asymp.	Stroke	Group 1/2
All		1121	991(88.4%)	108(9.6%)	65 / 27
50-69	<50	198	182(92%)	12(6.1%)	13 / 5
70-89	50-82	598	533(89.1%)	56(9.4%)	28 / 11
90-99	83-99	325	276(84.9%)	40(12.3%)	24 / 11

TIA's, transient ischemic attacks;

ECST, European Carotid Surgery Trial;

NASCET, North American Symptomatic Carotid Endarter. Trial

Images were initially statistically analyzed in order to identify if there is significant difference between the two groups and get an initial statistical model for classification of the two groups. Adaptive Network based Fuzzy Inference System (ANFIS) was used in order to create a model for automated classification of patients at long- or short-term stroke risk. The work is based on initial work published by the group in [15].

## II. METHODS

### A. Patient recruitment

Data used in this study were collected through the Asymptomatic Carotid Stenosis and Risk of Stroke study. Patients included in the study should be newly referred ( $< 3$  months), with 50-99% ICA stenosis in relation to the carotid bulb diameter (ECST method) without previous ipsilateral cerebral or retinal ischemic (CORI) symptoms and without neurological abnormalities. They were recruited to the study

after written informed consent. Patients who had had contralateral cerebral hemispheric/retinal or vertebrobasilar symptoms or signs of stroke/ transient ischemic attack (TIA) were included if asymptomatic for at least 6 months prior to recruitment. For patients with bilateral carotid atherosclerosis the side with the more severe stenosis was considered ipsilateral (the study artery) [2].

Data were collected at baseline when all patients were still asymptomatic; The data included duplex ultrasound scanning of the carotids. This was a procedure repeated at 6 months intervals until a primary endpoint or the end of the study was reached [2]. Duplex ultrasound scanning data were performed using a protocol and standard procedure specified during the study. These included artery stenosis and plaque characteristics based on image analysis algorithms. In addition to imaging several clinical data were collected. These included parameters like total cholesterol, LDL cholesterol, HDL cholesterol, Creatinine, Triglycerides etc. as published in [2][16].

TABLE II. MEAN, STANDARD DEVIATION AND PARAMETRIC TEST OF EQUALITY OF MEANS (SIG.) FOR THE THREE FEATURE SETS INVESTIGATED STROKE GROUPS: (1)  $\leq 3$  YEARS OF EVENT AND (2)  $> 3$  YEARS OF EVENT.

Group	Group 1	Group 2	Sig.
<b>Feature Set 1 (FS1) Clinical and Plaque Feat. [2][16]</b>			
Sten(%ECST)	81.97±11.17	80.33±13.75	0.552
Log(GSM+40)	4.026±0.235	4.098±0.234	0.186
(Plq Area) <sup>1/3</sup>	3.936±0.758	4.172±0.647	0.159
DWAs	0.785±0.414	0.889±0.320	0.245
Hist TIA/Stroke	0.292±0.458	0.444±0.506	0.163
<b>Feature Set 2 (FS2) Texture Feat. SGLDM [2][16]</b>			
ASM	0.077±0.126	0.040±0.065	0.159
CON	57.23±62.33	45.02±29.34	0.334
COR	0.972±0.019	0.981±0.007	0.028
VAR	1089±820	1353±977	0.188
SAV	57.65±30.18	68.65±34.60	0.131
SVA	4300±3247	5367±3885	0.180
SEN	4.437±0.985	4.77±0.658	0.111
ENT	6.10±1.49	6.60±0.981	0.107
DVA	36.79±42.66	27.21±18.78	0.266
DEN	2.26±0.504	2.38±0.290	0.228
InM1	-0.42±0.06	-0.41±0.03	0.342
InM2	0.97±0.03	0.98±0.01	0.131
<b>Feature Set 3 (FS3) Textur Feat. Runl FPS [2][16]</b>			
sqrnl	133.28±35.56	113.06±37.58	0.017
runl_SRE	0.909±0.033	0.894±0.022	0.026
fps_frad	3320±1432	2611±1549	0.038
fps_fang	2906±1301	2278±1411	0.043
runl_LRE	2.045±0.678	2.343±0.392	0.036
Runl_RP	23.26±10.13	17.71±13.55	0.033
<b>Feature Set 4 (FS4) Text Feat. Morphology [18]</b>			
L img cdf 1	0.020±0.023	0.016±0.017	0.442
L img cdf 2	0.057±0.064	0.052±0.048	0.685
L img cdf 3	0.103±0.109	0.094±0.071	0.694
L img cdf 4	0.146±0.141	0.141±0.091	0.854
L img cdf 5	0.190±0.167	0.187±0.112	0.935
L img pdf 1	0.020±0.023	0.016±0.017	0.442
L img pdf 2	0.037±0.042	0.035±0.032	0.842
L img pdf 3	0.046±0.046	0.042±0.027	0.725
L img pdf 4	0.043±0.034	0.046±0.026	0.628
L img pdf 5	0.044±0.033	0.046±0.029	0.727

\* SIGNIFICANTLY DIFFERENT MEANS ( $P < 0.05$ ) WITH PARAMETRIC TEST FOR TWO INDEPENDENT SAMPLES

The total number of patients collected through the study was 1121 out of which 108 strokes or TIAs were recorded. The characteristics of the different groups are shown in Table I. In the present study we had used data from subject that had Stroke and TIA events. These were further divided into two groups of patients, those that had an event in  $\leq 3$  years from baseline called short term group (group 1) and those that had an event in  $> 3$  years from baseline called long term group (group 2).

### B. Feature sets:

The feature sets extracted using image analysis as well as the clinical data sets were used in order to create and test the classification model. The image analysis features were also presented in previous studies [16], [17] and used for the classification of asymptomatic versus symptomatic patients.

Image analysis features were computed using the "Plaque Texture Analysis software" by LifeQ medical (<http://www.lifeqmedical.com/>). The standardization of images was done using an image normalization protocol as documented in [2][17].

The image analysis algorithms used for this study namely were the:

1) Statistical Features (SF) [2], [16] (see Table II, Feature Set1 - FS1). Stenosis based on ECST, logarithmic value of Gray Scale Media plus forty ( $\log(\text{GSM}+40)$ ), cubic root of the total plaque area (Plaque area) $^{1/3}$ , presence of discrete white areas on plaques(DWA), history of contralateral TIA and/or Stroke.

2) Spatial Gray Level Dependence Matrices (SGLDM) features [16], [17] (see Table II, Feature Set 2 - FS2). Angular second moment (ASM), contrast (CON), correlation (COR), variance (VAR), sum average (SAV), sum variance (SVA), sum entropy (SEN), entropy (ENT), difference variance (DVA), difference entropy (DEN), information measures 1 & 2 (InM1, InM2).

3) Features based on Run Length Statistics Algorithm [16], [17]. (see Table II, Feature Set 3 – FS3) Short Run Emphasis (SRE), Long Run Emphasis (LRE), Run Percentage (RP). Fourier Power Spectrum Angular (Fang) and Radial (Frad) power.

4) Additionally, plaque multiscale morphology features were extracted as described in [18] (see Table II, Feature Set 4 – FS4). This method leads to the consideration of morphological features that come from: (i) dark regions associated with lipid, thrombus, blood, or haemorrhage, (ii) bright regions associated with collagen and calcified components, and (iii) medium-brightness regions that fall between them as discussed in [18]. The morphological probability density function (L-pdf) and the cumulative distribution function (L-cdf) for several radii of the structural element and for the low images created using a multiscale morphological decomposition, were calculated and used in this study.

### C. Feature Selection:

Features used with SVM classifier were selected based on the statistical analysis and results presented in studies [16], [17]. While the features used with ANFIS were selected with the G-flip algorithm. G-flip algorithm is type of greedy search algorithm that depends on maximizing the evaluation function  $e(F)$ , where  $F$  is a set of features. The

algorithm repeatedly iterates over the feature set and updates the set of chosen features. In each iteration it is decided to remove or add the current feature to the selected set by evaluating the margin term in the equation 1 with and without this feature. The following equation shows the evaluating function for a training set  $S$  and a weight vector  $w$  according to the second definition of the margin in

$$e(w) = \sum_{x \in S} \Theta_{s/x}^w(x) \quad (1)$$

This algorithm converges to a local maximum of the evaluation function, as each step increases its value and the number of possible feature sets is finite. The computational complexity of one pass over all features of Gflip is

$$\Theta(N^2 m^2) \quad (2)$$

where  $N$  is the number of features and  $m$  is the number of instances. Empirically G-flip converges in a few iterations and there is no need to tune the number of features or any type of threshold [22].

### D. Risk Modelling

Risk modeling was carried out using Adaptive Network based Fuzzy Inference System (ANFIS) [23]. The model was investigated to classify the patients into two classes: (i) short term stroke ( $\leq 3$  years of event) and (ii) long term stroke (including TIA's) ( $> 3$  years of event).

The ANFIS structure is composed of five layers and it [23] is demonstrated in Fig. 2. The first layer executes a fuzzification process, the second layer executes the fuzzy and the antecedent part of the fuzzy rules, the third layer normalizes the membership functions (MFs), the fourth layer executes the consequent part of the fuzzy rules and the fifth layer computes the output of the fuzzy system by summing up the outputs of the fourth layer.

The feed forward equations of ANFIS are as follows:

$$w_i = \mu_{A_i}(x) \times \mu_{B_i}(y), \quad i = 1, 2 \quad (4)$$

$$\bar{w}_i = \frac{w_i}{w_1 + w_2}, \quad i = 1, 2 \quad (5)$$

$$f = \frac{w_1 f_1 + w_2 f_2}{w_1 + w_2} = \bar{w}_1 f_1 + \bar{w}_2 f_2 \quad (6)$$

Where  $f_1 = p_1 x + q_1 y + r_1 z$ ,

$$f_2 = p_2 x + q_2 y + r_2 z \quad (7)$$

In order to model complex nonlinear systems, the ANFIS model carries out input space partitioning that splits the input space into many local regions from which simple local models (linear functions or even adjustable coefficients) are employed. The ANFIS uses fuzzy MFs for splitting each input dimension. The input space is covered by MFs which are overlapping; that means several local regions can be activated simultaneously by a single input.

As simple local models are adopted in ANFIS model, the ANFIS approximation ability will depend on the resolution of the input space partitioning, which is determined by the number of MFs in ANFIS and the number of layers. Usually, MFs are used as bell-shaped with maximum equal to 1 and minimum equal to 0 such as [23].

ANFIS as Fuzzy Inference system the number of inputs must be avoid the curse of dimensionality situation. In such

situation the number of fuzzy rules increases exponentially with the number of inputs variable. To avoid the curse of dimensionality best features are selected by Greedy feature flip (G-flip) features selection algorithm.

### III. RESULTS

A group of 92 patients that had stroke or TIA were analyzed (16 patients were excluded due to missing clinical features (FS1)). Stroke patients consisted of two groups:

1. group 1 of 65 patients that had stroke  $\leq$  3 years from baseline, and
2. group 2 of 27 patients that had stroke  $>$  3 years from baseline.

The following feature sets (FS) were computed for the two groups of stroke patients as given in Table II:

- FS 1: ACSRS Clinical and plaque features: stenosis (%ECST),  $\log(\text{GSM}+40)$ ,  $(\text{plaque area})^{1/3}$ , DWA absent or present, and history of contralateral TIAs and/or Stroke.
- FS 3: Texture Features – SGLDM: SGLDM Spatial Gray Level Dependence Matrices - ASM, CON, COR, VAR, SAV, SVA, SEN, ENT, DVA, DEN, InM1, InM2.
- FS 3: ACSRS additional texture features as concluded from the statistical analysis: Run1\_SRE, Run1\_RP, Run1\_LRE, Fps\_fang, Fps\_frad.
- FS 4: Texture Features – Morphology: Low image cdf 1-5, and pdf 1-5.

### IV. DISCUSSION

Use of ultrasound imaging in defining stroke risk in asymptomatic patients has been presented through several studies [1], [2], [3], [5], [12], [13]. Despite the large number of publications, visual evaluation of plaques has several limitations and the acquisition procedure must be according to a predefined protocol in order to achieve the anticipated results **Hata! Başvuru kaynağı bulunamadı..** Several researchers are currently discussing non-surgical interventions for reducing stroke risk and prevention of possible stroke events [7] - [9]. The ultrasonic appearance of carotid plaques was proved a good predictor for stroke events [3], [11]. Despite the simplicity of calculation features like the Gray Scale Median of a plaque [5] have shown high significance on the estimation of the risk of stroke. Additionally, features applied for vision analysis (texture or shape morphology) proved to give some extra information on the final estimation of stroke risk [12][16]. All the above conclude that the prediction of risk is important as it will aid clinicians in the selection of asymptomatic cases at higher risk. Equally important is the establishment of a method that will allow for objective and quantitative evaluation of high-risk cases, that are the ones that would most benefit from endarterectomy.

Despite all these and according to our knowledge no study presented asymptomatic patients risk estimation correlated with time period. Based on the statistical analysis of the data collected through the ACSRS study [2]; the effort of this work was on the development of predictive modeling to identify groups of patients that are at high risk of stroke in a short term period ( $\leq$  3 years) as opposed to groups of patients that are at a high risk of stroke in long term ( $>$  3

years). This threshold was selected based on the initial statistical analysis of the data. Estimation of short versus long term risk can give physicians time for medical intervention except from surgery. Several ultrasound image analysis features as well as clinical features. The statistical analysis showed that the significant difference was better supported from the same features used for stroke versus asymptomatic patients estimation [2][12][16]. Simple features like the Gray Scale Median, the area of the plaque, the presence of discrete white areas in the plaque [17] proved to give very good classification results. The combination with classical texture features like the SGLDM and morphological features was able to improve the overall performance at a percentage of 97% when using the ANFIS. The introduction of a classification model called Adaptive Network based Fuzzy Inference System (ANFIS) ended to a very promising result for this feature set. Based on these we can see that these features can be used as an indicator for the estimation stroke risk as long (more than 3years) or short time (less or equal than 3 years).

### V. CONCLUSIONS:

For the first time we are showing that the stroke risk can be divided into groups of short-term groups, less or equal to three years and long term group, more than three years. The data used were collected from the ACSRS study where monitoring of the patients started when they were still asymptomatic and continued up to a period of 8 years. The predictive model is based on ANFIS classifiers. We had used several clinical feature sets recorded during the ACSRS study as well as features extracted from the images of the study. The results are very encouraging, and they are consistent with results presented by the group and other researchers in previous studies that were dealing with the identification of asymptomatic versus symptomatic plaques. We anticipate that the combination of these results with analysis of data from real time ultrasound video could become a significant tool, which could support the decision AND URGENCY for carotid plaque surgery.

### CONTRIBUTION OF THE AUTHORS

The contributions of the authors to the article are equal.

### CONFLICT OF INTEREST

There is no conflict of interest between the authors.

TABLE III. SHORT TERM AND LONG TERM STROKE RISK ANFIS PREDICTIVE MODELLING EVALUATION RESULTS (COMPUTED BASED ON 10 RANDOM SETS OF 40 PATIENTS EACH WHERE THE EVALUATION WAS CARRIED OUT USING LEAVE ONE OUT METHOD FOR EACH SET). FEATURES SETS WERE USED AS TABULATED IN TABLE II.

FS1	FS2 - Selected	FS3	FS4	FS5 - Selected	Classifier	Correct classification	Sensitivity	Specificity
+					A	95.44 $\pm$ 0.40	95.00 $\pm$ 0.8	95.87 $\pm$ 0.8
	+				A	96.58 $\pm$ 0.92	95.00 $\pm$ 1.85	98.15 $\pm$ 1.85
		+			A	97.43 $\pm$ 2.57	97.50 $\pm$ 2.34	97.36 $\pm$ 2.64
			+		A	92.44 $\pm$ 7.56	92.94 $\pm$ 8.05	91.95 $\pm$ 8.05
				+	A	96.12 $\pm$ 0.66	95.00 $\pm$ 1.32	97.25 $\pm$ 1.32

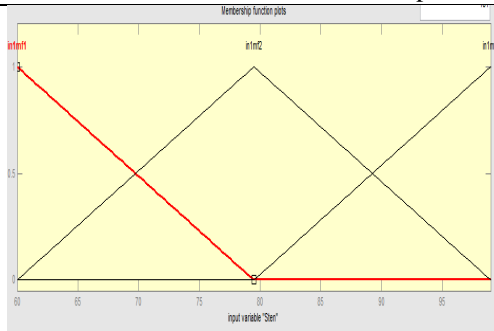


Fig. 2. Three Inputs member functions (MFs are generalized triangular by three parameters)

#### STATEMENT OF RESEARCH AND PUBLICATION ETHICS

Research and publication ethics were observed in this study

#### REFERENCES

- [1] A. Fox, "How to Measure Carotid Stenosis", *Radiology*, vol.186, pp.316-318, 1993.
- [2] A. Nicolaides, S. Kakkos, E. Kyriacou, M. Griffin et al. "Asymptomatic Internal Carotid Artery Stenosis and Cerebrovascular Risk Stratification," *Journal of Vascular Surgery*, vol.52, no.4 pp.1486-1496, Dec. 2010.
- [3] Executive Committee for the Asymptomatic Carotid Atherosclerosis Study, "Endarterectomy for asymptomatic carotid artery stenosis," *J. Am Med Assoc*, vol.273, pp.1421-8, 1995.
- [4] MRC Asymptomatic Carotid Surgery Trial (ACST) Collaborative Group, "Prevention of disabling and fatal strokes by successful carotid endarterectomy in patients without recent neurological symptoms: randomized controlled trial," *Lancet*, vol.363, pp.1491-502, 2004.
- [5] E. Mathiesen, K. Bonan, O. Joakimsen, "Echolucent Plaques Are Associated With High Risk of Ischemic Cerebrovascular Events in Carotid Stenosis: The Tromso Study", *Circulation*, vol.103, pp.2171-2175, 2001.
- [6] A.L. Abbott and G.A. Donnan, "Does the 'High Risk' Patient with Asymptomatic Carotid Stenosis Really Exist?", *European Journal of Endovascular Surgery*, vol.35, pp.524-533, 2008.
- [7] A.R. Naylor, P.A. Gaines, P.M. Rothwell, "Who benefits most from intervention in asymptomatic carotid stenosis: patients or professionals?" *Eur J Vasc Endovasc Surg*, vol.37, pp.625-32, 2009.
- [8] A. Abbott, "Asymptomatic carotid artery stenosis – it's time to stop operating", *Nature Clinical Practice Neurology*, vol.4, pp.4-5, 2008.
- [9] A. Abbott, "Medical (Nonsurgical) Intervention Alone Is Now Best for Prevention of Stroke Associated With Asymptomatic Severe Carotid Stenosis: Results of a Systematic Review and Analysis", *Stroke*, vol.40, pp.573-583, 2009.
- [10] M. Reiter, R. Horvat, S. Puchner, W. Rinner, P. Polterauer, J. Lammer, E. Minar, R.A. Bucek, "Plaque Imaging of the Internal Carotid Artery – Correlation of B-Flow Imaging with Histopathology", *American Journal of Neuroradiology*, vol.28, pp.122-126, 2007.
- [11] R. Topakian, A. King, S. Kwon, A. Schaafsma, M. Shipley, H. Markus, "Ultrasonic plaque echolucency and emboli signals predict stroke in asymptomatic carotid stenosis", *Neurology*, vol.77, pp.751-758, 2011.
- [12] R. Doonan, J. Gorgui, J. Veinot, C. Lai, E. Kyriacou, M.M. Corriveau, O. Steinmetz, K. S.S. Daskalopoulou "Plaque Echodensity and Textural Features are Associated with Histologic Carotid Plaque Instability", *Journal of Vascular Surgery*, Vol. 64, No.3, pp 671-677, Sept. 2016.
- [13] A. AbuRahma, J. Wulu, B. Crotty, "Carotid plaque ultrasonic heterogeneity and severity of stenosis", *Stroke*, vol.33, pp.1772-1775, 2002.
- [14] A.L. Leahy, P.T. McCollum, T.M. Feeley et al., "Duplex ultrasonography and selection of patients for carotid endarterectomy: Plaque morphology or luminal narrowing?", *Journal of Vascular Surgery*, vol.8, pp.558-62, 1998.
- [15] E. Kyriacou, P. Vogazianos, et al., Prediction of the Time Period of Stroke based on Ultrasound Image Analysis of Initially Asymptomatic Carotid Plaques, in Proc. of 37th Annual Conference of the IEEE Engineering in Medicine and Biology Society (EMBC), Milano, Italy, Aug. 25 – 29, pp. 334-337, 2015.
- [16] E.C.Kyriacou, S.Petroudi, C.S.Pattichis, M.S.Pattichis, M.Griffin, S. Kakkos, A.Nicolaides, "Prediction of High Risk Asymptomatic Carotid Plaques Based on Ultrasonic Image Features," *IEEE Transactions on Information Technology in Biomedicine*, Vol. 16, no.5, pp.966-973, 2012.
- [17] S.K. Kakkos, J.M. Stevens, A.N. Nicolaides, E. Kyriacou, C.S.Pattichis, G. Geroulakos, D. Thomas, "Texture Analysis of Ultrasonic Images of Symptomatic Carotid Plaques Can Identify Those Plaques Associated with Ipsilateral Embolic Brain Infarction," *European Journal of Vascular and Endovascular Surgery*, vol.33, no.4, pp.422-429, 2007.
- [18] E. Kyriacou, M.Pattichis, C.S. Pattichis, A. Mavrommatis, C.I. Christodoulou, S. Kakkos, A. Nicolaides, "Classification of Atherosclerotic Carotid Plaques Using Morphological Analysis on Ultrasound images," *J. of Applied Intell.*, Springer, vol.30, no.1, pp.3-23, 2009.
- [19] H. Ma, A.I. Bandos, H.E. Rockette, and D. Gur, "On use of partial area under the ROC curve for evaluation of diagnostic performance," *Stat. In Medicine*, vol.32, no.20, pp. 3449-3458, 2013.
- [20] V. Vapnik, S. Golowich, A. Smola, "Support vector method for function approximation, regression estimation, and signal processing", *Advances in Neural Information Process. Systems 9*, Morgan Kaufmann, pp. 281–287, 1997.
- [21] C. C. Chang, C. J. Lin. "LIBSVM: A library for support vector machines", *ACM Trans. Intellig. Syst. & Techn.*, vol. 2, no. 3, 2011. (Software available at: <http://www.csie.ntu.edu.tw/~cjlin/libsvm>).
- [22] R. Gilad-Bachrach, A. Navot and N. Tishby, "Margin based feature selection - theory and algorithms," In *ICML 2004*, 4-8 July 2004, Banff, Canada
- [23] S. H. Kim, Y. H. Kim, K. B. Sim, H. T. Jeon, "On Developing an adaptive neural-fuzzy control system," *Proceeding of IEEE/RSJ Conference on intelligent robots and systems Yokohama, Japan*, July 1993 pp 950-957.